Received: 15 May 2016 | Accepted: 10 December 2016

DOI 10.1002/hyp.11105

WILEY

RESEARCH ARTICLE

Characteristics of soil water movement in a grass slope in a karst peak-cluster region, China

Wei Liu[1,2,3] | Shijie Wang[2,4] | Weijun Luo[2,4] | Weiwei Dai[3] | Edith Bai[3]

[1] College of Environment and Safety Engineering, Shenyang University of Chemical Technology, Shenyang 110142, China

[2] State Key Laboratory of Environmental Geochemistry, Institute of Geochemistry, Chinese Academy of Sciences, Guiyang 550081, China

[3] CAS Key Laboratory of Forest Ecology and Management, Institute of Applied Ecology, Chinese Academy of Sciences, Shenyang 110164, China

[4] Puding Karst Ecosystem Research Station, Chinese Academy of Sciences, Puding 562100, China

Correspondence
Shijie Wang, State Key Laboratory of Environmental Geochemistry, Institute of Geochemistry, Chinese Academy of Sciences, Guiyang 550081, China.
Email: wangshijie@vip.skleg.cn

Funding information
National Key Basic Research Program of China, Grant/Award Number: 2013CB956700. National Key Research Program of China, Grant/Award Number: 2016YFC0502300. 2016YFC0502602. NSFC-RCUK_NERC project, Grant/Award Number: 41571130074. National Natural Science Foundation of China, Grant/Award Number: 41603001.

Abstract

Soil water is very important in hilly areas with thin soil layers and deep groundwater tables, such as the karst peak-cluster region of Southwest China. An investigation into soil water movement can provide insights into management of shallow water resources and soil nutrients, as well as prevention of groundwater pollution. In this study, ^{18}O and ^{2}H tracers were used to trace soil water movement in planar soil mass type microhabitats in the middle part of a steep hillslope covered by grasses in a karst peak-cluster region of China. From May 2008 to July 2009, samples of precipitation and two types of soil water, which had different integrated degrees of mobility and were of different depth intervals or depths, were collected. The hydrogeochemical characteristics were compared between precipitation and soil water, and these data were applied in convolution-based lumped parameter models. Our results indicated that vertical piston flow, rather than lateral flow along the soil–bedrock interface, played an important role in soil water percolation at least in the upper soil layer approximately 7 cm over the permeable bedrock. The mixing effect and preferential flow might also play a role in soil water percolation. In general, the evaporation effect on soil water was weak except for the uppermost 10 cm soil matrix water during winter. The lower limits of mean transit time of soil matrix flow passing through 5, 15, 25, 35, and 41.5 cm depths were 4.81, 7.70, 16.19, 21.85, and 27.44 days, respectively. Our study demonstrated the crucial functions of the soil reservoir in regulating the water cycle and could provide guidance on conservation of soil water and hydrological studies. The applied method was proved to be a suitable approach for investigating soil water movement on a monthly scale.

KEYWORDS

hydrogen and oxygen isotopes, mean transit time, piston flow, preferential flow, soil water

1 | INTRODUCTION

Soil water is very important in hilly areas with thin soil layers and deep groundwater tables, such as the karst peak-cluster region (KPCR)[1] of Southwest China. An investigation into soil water movement is a prerequisite for hydrological, hydrochemical, and ecohydrological studies (Gazis & Feng, 2004; Mueller et al., 2014) and can provide insights into the management of water resources and soil nutrients, as well as the prevention of groundwater pollution.

Soil water movement may be upward (evaporation and transpiration) or downward (percolation, lateral flow, etc.). ^{18}O and ^{2}H are ideal tracers of water movement. Due to the effects of temperature and precipitation amount, and changes in the origin of precipitation-producing air masses, among other effects, the $\delta^{18}O$ ($\delta^{2}H$) value of

A list of acronyms and shortened phrases (in alphabetical order): (shortened as convolution model), convolution-based lumped parameter model; (DM), dispersion model; (EM), exponential model; (EPM), exponential-piston flow model; (KPCR), karst peak-cluster region; (LMWL), local meteoric water line; (LL_{MTT}), lower limit of the mean transit time; (MPR), mean percolation rate; (MTT), mean transit time; (shortened as mobile flow), more mobile soil water flow; (PFM), piston-flow model; (shortened as planar soil microhabitat), planar soil mass type microhabitat; (SMF), soil matrix flow; (SVWC), soil volumetric water content; (RMSE), square root of the mean square error; (TSPW), total soil pore water; (TTDF), transit time distribution function; (V-SMOW), Vienna standard mean ocean water

[1] KPCR is characterized by a karst peak-cluster landscape that is developed from intensive karstification of soluble carbonate rock (e.g., limestone and dolostone) and has a cluster of lofty cone-shaped peaks interconnected at their bottoms. The relative peak heights are approximately 300 to 600 m, and their slope gradients are 30° to 60°.

precipitation (an important source of soil water) for a given region generally changes distinctly with time (Dansgaard, 1964; Gat, Mook, & Meijer, 2001; Vuille, Werner, Bradley, & Keimig, 2005). Unlike water phase transitions, soil water percolation and water uptake by plant roots are generally non-isotope-fractionating processes (Brunel, Walker, & Kennett-Smith, 1995; Dawson & Ehleringer, 1991; Dawson & Ehleringer, 1993; Ehleringer & Dawson, 1992; Walker & Richardson, 1991). Due to the physical and chemical similarities of water isotopologies ($^1H_2{}^{16}O$, $^1H^2H^{16}O$, $^1H_2{}^{18}O$, etc.), ^{18}O and ^2H tracers overcome the limitations of other tracers, such as adsorption or desorption, dissolution or precipitation, and ion interaction effects (Barnes & Allison, 1988; Williams, 1997). They can be used to estimate evaporation rates (Allison & Barnes, 1983; Barnes & Allison, 1988; Shanafield et al., 2015), trace plant water sources (Dai, Zheng, Tang, & Li, 2015; Wang, Song, Han, Zhang, & Liu, 2010; Yang, Wen, & Sun, 2015), partition evapotranspiration into evaporation and transpiration (Brunel, Walker, Dighton, & Monteny, 1997; Dubbert, Cuntz, Piayda, Maguás, & Werner, 2013; Wang & Yakir, 2000), reveal percolation mechanisms (e.g., piston flow or preferential flow) (Gazis & Feng, 2004; Stumpp & Hendry, 2012), mean transit times (MTTs) of soil water (Adomako, Maloszewski, Stumpp, Osae, & Akiti, 2010; Stumpp, Maloszewski, Stichler, & Fank, 2009a; Stumpp, Nützmann, Maciejewski, & Maloszewski, 2009b; Stumpp, Stichler, & Maloszewski, 2009c; Stumpp, Stichler, Kandolf, & Šimůnek, 2012), etc. The transit time reflects flow pathways, water storage, and sources in a single index (McGuire & McDonnell, 2006). Several simple black box models, especially convolution-based lumped parameter models (hereafter referred to as convolution models; Lee, Kim, Lee, Kim, & Lee, 2007; Małoszewski & Zuber, 1982; McGuire & McDonnell, 2006; Stumpp, Maloszewski, Stichler, & Fank, 2009a; Stumpp, Nützmann, Maciejewski, & Maloszewski, 2009b), have been developed to estimate MTTs of subsurface flow. Some convolution models have been verified to be applicable to the unsaturated zone, because they yielded estimates of transport parameters that were similar to those of a physically based numerical model (Stumpp & Maloszewski, 2010; Stumpp, Maloszewski, Stichler, & Fank, 2009a; Stumpp, Nützmann, Maciejewski, & Maloszewski, 2009b; Stumpp, Stichler, & Maloszewski, 2009c).

Several techniques have been developed to determine the $\delta^{18}O$ and δ^2H values of different portions of soil water that have different integrated degrees of mobility. Soil water can be extracted by in situ samplers—for example, zero-tension lysimeters (McGuire, DeWalle, & Gburek, 2002), wick samplers (Landon, Delin, Komor, & Regan, 1999), and suction lysimeters (DeWalle, Edwards, Swistock, Aravena, & Drimmie, 1997)—soil core collection and subsequent centrifugation (Figueroa-Johnson, Tindall, & Friedel, 2007), vacuum distillation (West, Patrickson, & Ehleringer, 2006), or azeotropic distillation (Ingraham & Shadel, 1992). Its $\delta^{18}O$ and δ^2H values can then be determined by an isotope ratio mass spectrometer or a laser-based water vapor isotope analyzer (Sturm & Knohl, 2010; Wang, Caylor, & Dragoni, 2009). The distillation methods can extract almost all total soil pore water (TSPW), whereas other methods can extract only different portions of TSPW, which are positively correlated with the applied suction or centrifugal force. Alternatively, the isotopic composition of soil water can be analyzed based on direct equilibration of TSPW with CO_2 (for $\delta^{18}O$ analysis; Allison, Colin-Kaczala, Filly, & Fontes, 1987; Hsieh, Savin, Kelly, & Chadwick, 1998) or water vapor (for $\delta^{18}O$ and δ^2H analysis) (Rothfuss, Vereecken, & Brüggemann, 2013; Volkmann & Weiler, 2014). More recently, new techniques have been developed for continuous automatic in situ monitoring of soil water $\delta^{18}O$ and δ^2H values (Rothfuss, et al., 2013; Volkmann & Weiler, 2014), with the potential to improve our understanding of soil water movement over short timescales. Several studies found that different portions of TSPW collected by different methods had different $\delta^{18}O$ and δ^2H values (Figueroa-Johnson et al., 2007; Landon et al., 1999), verifying that different techniques might measure different portions of soil water that had different integrated degrees of mobility (Gazis & Feng, 2004). Thus, a combination of different soil water collection techniques has the potential to give more information about water movement.

In karst regions of Southwest China, intensive karstification generally results in extensive development of solutionally enlarged fractures, karst caves, and underground rivers, and so forth, in the bedrock, leading to rapid drainage of surface water to deep groundwater systems (Yuan, 1997). Due to the shallow or even discontinuous soil layer (Cao, Yuan, & Pan, 2003; Sun, Wang, Liu, & Feng, 2002) and the rapid drainage of surface water, soil water is scarce and is a limiting factor in these areas. Many studies have been conducted here to investigate soil water characteristic curves (Jiang et al., 2006; Li, Chen, Zhou, & Fang, 2008; Li, Gao, Wei, Xie, & Liu, 2003), infiltration rates (Dang, Chen, & Ma, 2012; Zhang, Zhu, Wang, Fu, & Wen, 2010), and spatiotemporal variations in the soil water content (Liu, Jiang, Liu, Xiao, & Xia, 2005; Zhang, Chen, Su, Zhang, & Kong, 2008; Zhang et al., 2014a). However, to the best of our knowledge, no study has been carried out in these regions to reveal soil water movement characteristics.

Here, at the center of the karst regions of Southwest China, we studied characteristics of soil water movement in the middle part of a steep hillslope in a KPCR. The main objectives are as follows: (1) to trace soil water percolation by comparing temporal and vertical variations in $\delta^{18}O$ (δ^2H) values of soil water collected by soil core collection–vacuum distillation with temporal variation in rainfall $\delta^{18}O$ (δ^2H) values; (2) to determine MTTs of soil matrix flow (SMF) passing through five different depths based on convolution modeling; and (3) to preliminarily explore characteristics of more mobile soil water flow (hereafter referred to as mobile flow) by comparing hydrogeochemical characteristics of soil water collected by zero-tension lysimeters with those of rainfall. We wanted to verify if synchronous hydrogeochemical monitoring of different portions of soil water could complement each other to give more information about soil water movement. We also tried to improve the accuracy of the fitted transport parameter(s) of the convolution model through modifications of the input, weighting, and output functions via elimination of the relatively stagnant periods of the intermittent soil water flow for the time variable. It is hoped that this research would not only provide insights into management of water resources and prevention of groundwater pollution in KPCRs but also provide guidance on soil water movement studies in other areas.

2 | SITE DESCRIPTION

This study was conducted in the Maolan National Nature Reserve of Libo Country in Guizhou Province of China. With a typical peak cluster landscape (Figure 1), the study area is tectonically located between the axes of the north-northeast-trending Weng'ang anticline and Maolan syncline. The strata, slightly dipping to the east, are composed of light gray to gray, thick-stratified to massive, and fine- to middle-grained dolomite of the Baizuo Formation (lower carboniferous) occasionally intercalated with limestone (Mao & Zhang, 1987). The bedrock is highly fractured and karstified. A study site in the middle of a steep hillslope was selected to trace soil water movement (Figures 1 and 2). More than 90% of the hillslope is covered by grasses of 0.5 to 1 m in height, with *Heteropogon contortus*, *Arthraxon prionodes*, *Pteridium revolutum*, *Dicranopteris dichotoma*, and *Miscanthus floridulus* as dominant species, while the rest is mainly covered by approximately 1.5-m-tall shrubs. The soil layer is generally thin and discontinuous. Due to complex micro-topographies of both soil and bedrock surfaces in KPCRs, several types of microhabitats, such as the planar soil mass type microhabitat (hereafter referred to as planar soil microhabitat), the gully-shaped soil mass type microhabitat, the crevice-shaped soil mass type microhabitat, and the planar bare rocky surface type microhabitat, can be identified (Liao, Long, Li, Yang, & Feng, 2012; Liu, Wang, Luo, Liu, & Liu, 2008; Wang, Lu, Zhou, Xie, & Da, 2007). Planar soil microhabitats are widespread in KPCRs, and soil water movement in such a microhabitat was investigated in this study. A typical planar soil microhabitat has a surface area of approximately 10 to 30 m^2, a very thin litter layer, and a 20- to 80-cm (generally less than 50 cm) thick soil layer whose depth-to-width ratio is usually less than 0.5. Soil water was collected approximately 2.24 km away from the rainfall collection site in Laqiao Village (Figure 1).

The study area has an East Asia humid mid-subtropical monsoon climate. The mean annual precipitation is 1,653 to 1,752 mm, with approximately 81% falling in the monsoonal rainy season between April and September. The mean annual temperature is 14.4 to 15.3 °C. The mean annual relative humidity is above 83% (Gan & Mu, 1987).

3 | METHODS

3.1 | Sampling

From May to June 2008, we excavated three typical soil profiles at three planar soil microhabitats. Three sets of 100 cm^3 intact soil samples were collected from 2.5 to 7.5, 12.5 to 17.5, 22.5 to 27.5, 32.5 to 37.5, and 39 to 44 cm depth intervals, for soil bulk density analysis. Another three sets of composite soil samples were collected from 0 to 10, 10 to 20, 20 to 30, 30 to 40, and 40 to 50 cm depth intervals, for soil texture analysis.

From May 2008 to July 2009, rainfall and soil water samples were collected to determine their $\delta^{18}O$ and $\delta^{2}H$ values.

Rainfall samples were collected by a standard rain gauge installed in Laqiao Village (Figure 1). After each rainfall event, a rain water

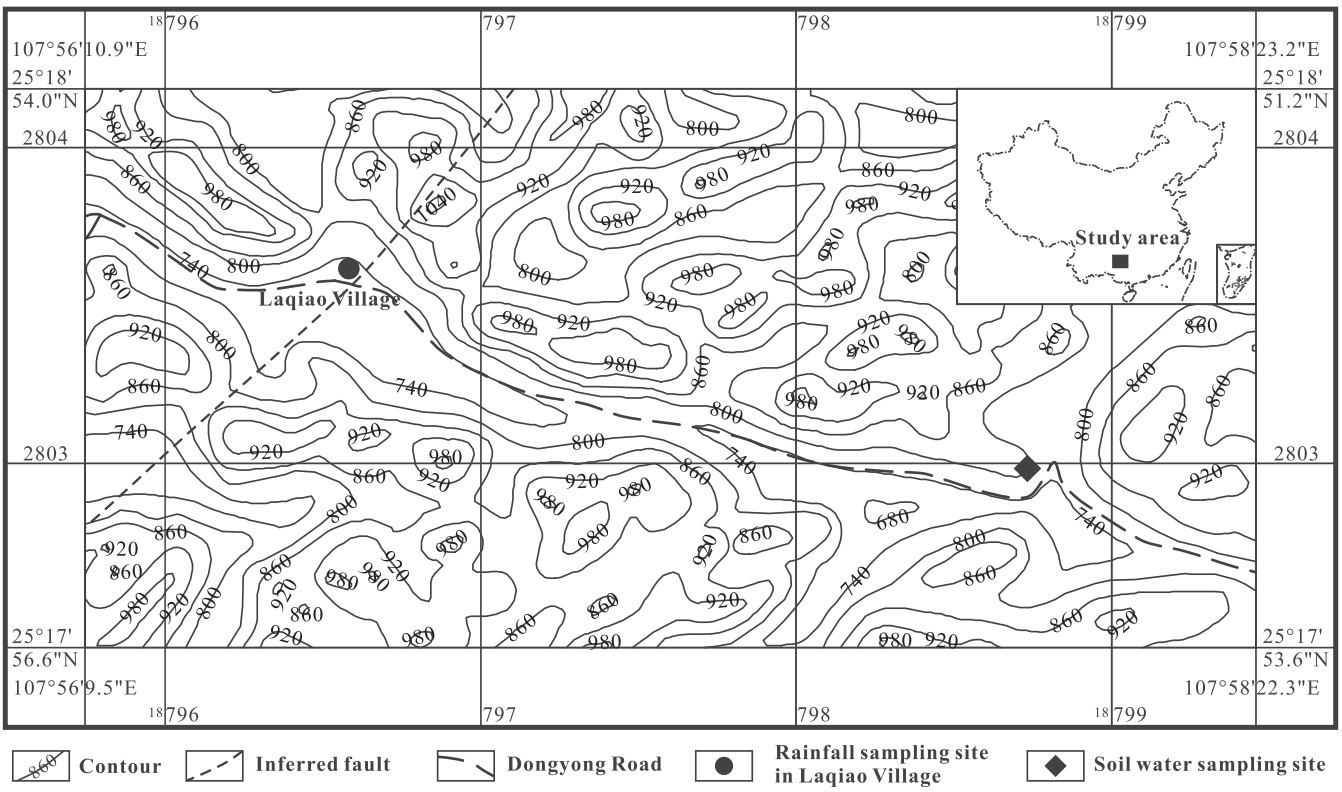

FIGURE 1 Sketch map showing topographic features of the study area and the sampling locations of soil water and rainfall. The projection was Xian_1980_GK_CM_105E (Xian 1980 6-degree gauss-kruger transverse Mercator 105 E [Zone 18]), with Yellow Sea 1985 as the vertical coordinate system

FIGURE 2 A photograph of the soil water sampling site and a typical soil profile in the planar soil mass type microhabitat (as an inset in the lower right). In the microhabitat, the soil thickness is approximately 20 to 80 cm (generally less than 50 cm), and the soil color gradually changes from black to yellow brown (or brown yellow) with soil depth

sample was stored in a 15-ml glass vial as soon as possible and then was preserved at 4 °C until analysis. The rainfall amount was recorded at the same time. No snow event occurred during the study period.

Soil water samples were collected by both soil core collection–vacuum distillation and the zero-tension lysimetric method. For the former method, soil core samples were collected from planar soil microhabitats and were then used as soon as possible to extract soil water samples by vacuum distillation according to the procedures proposed by West et al. (2006). For each soil sampling campaign, three 43-cm depth soil columns were simultaneously collected from three random planar soil microhabitats, and then each column was cut into one 3-cm piece and four 10-cm pieces from the bottom to the top. The soil column pieces of the same depth interval were well mixed in situ as soon as possible, and then the composite sample was partly stored in a 25-ml glass bottle and frozen until distillation. The soil water samples extracted by vacuum distillation were stored in 5-ml glass vials and preserved at 4 °C until analysis. Soil samples were weighed before and after distillation to calculate the gravimetric water content. Hereafter, soil water extracted by this method is called I-type soil water, with I_1, I_2, I_3, I_4, and I_5 representing I-type soil water from 0 to 10, 10 to 20, 20 to 30, 30 to 40, and 40 to 43 cm depth intervals, respectively. Because the vacuum distillation method can extract almost all mobile water and even some immobile water weakly bound to clay minerals from the soil sample (Araguás-Araguás, Rozanski, Gonfiantini, & Louvat, 1995), the hydrogeochemical signatures of I-type soil water can reflect the characteristics of soil water movement, provided that the soil clay content is low.

For the zero-tension lysimetric method, two typical planar soil microhabitats on locally gentle slopes, that is, Plots 1 and 2 (Figure 1), were selected to install zero-tension lysimeters. A zero-tension lysimeter is composed of a 400-cm^2 square polyethylene tray, a 2-L polyethylene bottle, a conducting tube connecting the tray and the bottle, a vent tube, and a sampling tube. The tray was inserted horizontally into the side wall of an excavated soil pit facing downslope to intercept water flow from the upper intact soil column. The distance between the side wall and the outermost edge of the tray was no less than 10 cm. The intercepted water was conducted to the bottle by gravity. During this process, the vent tube (extending from the top of the bottle to the soil beneath the tray) served as an air vent to prevent pressure changes in the bottle. The sampling tube extended from the bottom of the bottle to the surface. The excavated soil was backfilled into the soil pit and compacted after installation of the lysimeters. The highly fractured and karstified bedrock, the steep slope, the thin soil layer, and the deep groundwater table facilitated drainage of soil water in this study site. Therefore, although the backfilled soil was looser than the underlying non-excavated soil, the good drainage conditions inhibited the potential artificial lateral flow near the bottom of the backfilled soil block from reaching the collection tray installed at the upper position along the hillslope. From August to October 2007, five collection trays were installed into the same side wall of an excavated soil pit in Plot 1 at 10, 20, 30, 40, and 50 cm depths, while two were installed into the same side wall of another pit in Plot 2 at 30 and 50 cm depths. Until April 2008 (more than 6 months after the installation of the lysimeters), the amount of water collected from a deeper depth was not considerably larger than that from a shallower one in each plot. This phenomenon was further verified by the subsequent formal sampling of the lysimeters (details given in Section 4.3.2). Therefore, lateral flow, either artificial lateral flow near the bottom of the backfilled soil block or natural lateral flow along the soil–bedrock interface, was not an important water source for our lysimeters. For each formal sampling campaign, soil water in each storage bottle was extracted by a clean syringe until empty and then partly stored in a 15-ml glass vial and preserved at 4 °C until analysis. The volume of each sample was recorded at the same time. Hereafter, soil water collected by the lysimetric method is called II-type soil water, with II_1, II_2, II_3, II_4, and II_5 representing II-type soil water from 10, 20, 30, 40, and

50 cm depths, respectively. Due to the capillary barrier effect, a zero-tension lysimeter could collect leachate only when the soil above the tray was saturated. Therefore, during unsaturated soil water percolation, soil water would accumulate over the collection tray. In this case, the soil water potential over the tray would be larger than that surrounding the tray, and soil water flow would bypass the tray, leading to a low collection efficiency (Jemison & Fox, 1992; Peters & Durner, 2009; Zhu, Fox, & Toth, 2002). Once the soil over the tray was fully or partially saturated, mobile flow, especially preferential flow, would more readily drip into the tray. Therefore, the hydrogeochemical signatures of II-type soil water contained information about the characteristics of mobile flow.

Soil water samples of five consecutive depth intervals or depths with total depths larger than 43 cm were simultaneously collected monthly. Several short timescale sampling campaigns were also conducted, especially for II-type soil water. It is expected that synchronous monitoring of rainfall and soil water hydrogeochemical characteristics for at least one hydrological year is adequate for revealing the long-term trends of soil water movement characteristics in the study area.

3.2 | Analysis

All samples were analyzed in the State Key Laboratory of Environmental Geochemistry, Institute of Geochemistry, Chinese Academy of Sciences.

Particle size distributions of soil samples were analyzed by a laser particle size analyzer (Malvern Mastersizer 2000). Bulk densities of soil samples were measured by the oven-drying method at 105 °C for at least 8 hr. The soil volumetric water content (SVWC) was calculated by multiplying the gravimetric water content by the corresponding soil bulk density.

The isotopic composition of the water sample was analyzed by a multiflow continuous flow isotope ratio mass spectrometer (IsoPrime). The isotopic concentration was reported in the conventional δ notation relative to the Vienna standard mean ocean water (VSMOW) standard, according to the following equation:

$$\delta(‰) = \left(R_{\text{sample}}/R_{\text{VSMOW}} - 1\right) \times 10^3 \quad (1)$$

where R is the isotopic ratio $^{18}O/^{16}O$ or $^{2}H/^{1}H$. The analytical precision was ±0.2‰ for the $\delta^{18}O$ values and ±2‰ for the $\delta^{2}H$ values.

3.3 | Statistics

Regression analyses were performed using OriginPro 8 (Originlab Corporation, 2007).

3.4 | Convolution-based lumped parameter model

A detailed description of the convolution models and their applicability can be found in the literature (Amin & Campana, 1996; Jódar, Lambán, Medina, & Custodio, 2014; Małoszewski & Zuber, 1982; Małoszewski & Zuber, 1985; Małoszewski & Zuber, 1996; McGuire & McDonnell, 2006; Zuber, 1986a, 1986b; Zuber & Małoszewski, 2001), and only the knowledge most relevant to this study is briefly given below.

For a groundwater flow system with quasi-steady flow and the conservative isotope tracer, ^{18}O or ^{2}H, the output tracer can be related to the input tracer by the convolution integral (Małoszewski & Zuber, 1982; McGuire et al., 2002):

$$\delta_{\text{out}}(t) = \int_{-\infty}^{t} \delta_{\text{in}}\left(t'\right) g\left(t - t'\right) dt' \quad (2)$$

where $\delta_{\text{out}}(t)$ is the output $\delta^{18}O$ or $\delta^{2}H$ at time t, t' is an integration variable that describes the entry time to the system, t is the calendar time, $\delta_{\text{in}}(t')$ is the input function of $\delta^{18}O$ or $\delta^{2}H$ to the system, and $g(t-t')$ is the transit time distribution function (TTDF) of ^{18}O or ^{2}H, which is equivalent to the probability density of the tracer leaving the system for a single input (McGuire & McDonnell, 2006; Zuber, 1986a, 1986b).

To include a weighting of the input data in the simulation and assuming that each tracer input into the system has the same TTDF, we can modify Equation 2 as follows (Martinec, Siegenthaler, Oeschger, & Tongiorgi, 1974; Stewart & McDonnell, 1991; Weiler, McGlynn, McGuire, & McDonnell, 2003):

$$\delta_{\text{out}}(t) = \frac{\int_{-\infty}^{t} w\left(t'\right) \delta_{\text{in}}\left(t'\right) g\left(t - t'\right) dt'}{\int_{-\infty}^{t} w\left(t'\right) g\left(t - t'\right) dt'} \quad (3)$$

where $w(t)$ is the weighting function, which can include any appropriate factor, such as rainfall rates, throughfall rates and effective rainfall (McGuire & McDonnell, 2006).

There are four common model types defined by the TTDFs: piston-flow model (PFM)

$$g(t) = \delta(t - \tau) \quad (4)$$

exponential model (EM)

$$g(t) = \frac{1}{\tau} \exp\left(\frac{-t}{\tau}\right) \quad (5)$$

exponential-piston flow model (EPM)

$$g(t) = \frac{\eta}{\tau} \exp\left(-\frac{\eta t}{\tau} + \eta - 1\right) \text{ for } t \geq \tau\left(1 - \frac{1}{\eta}\right) \quad (6)$$

$$g(t) = 0 \text{ for } t < \tau\left(1 - \frac{1}{\eta}\right) \quad (7)$$

dispersion model (DM)

$$g(t) = \left(\frac{4\pi D_p t}{\tau}\right)^{-1/2} t^{-1} \exp\left[-\left(1 - \frac{t}{\tau}\right)^2 \left(\frac{\tau}{4 D_p t}\right)\right] \quad (8)$$

where τ is the MTT of the isotope tracer, η equals the sum of two volumes with the Dirac delta distribution and exponential distribution of transit times divided by the volume with the latter transit time distribution, and D_p is the apparent dispersion parameter, which equals the reciprocal of the Péclet number when vertical soil water movement through the vadose zone was modeled (Maloszewski & Zuber, 1996).

The TTDF of the tracer can be identified with that of water flow only under favorable conditions, which exist when there are no stagnant zones in the investigated system. Otherwise, even an ideal

tracer may be delayed with respect to the water flow due to diffusion exchange between mobile and immobile zones (Turnadge & Smerdon, 2014; Zuber & Małoszewski, 2001).

The downward soil water movement in the studied upper 43-cm soil layer was dominated by vertical percolation (details given in Section 5.1.2). After a heavy rainfall or irrigation event, the well-drained soil generally drains excess water within approximately 2 to 3 days until it reaches the field capacity, and then the downward water percolation becomes very slow (Veihmeyer & Hendrickson, 1931). In this study area, the highly fractured and karstified bedrock, the deep groundwater level, and the low soil-clay content (Table 1) facilitated fast drainage of soil water. It usually took less than 2 days for the upper 43 cm of soil to drain to the field capacity after a recharge event. The convolution model approach is most suitable for groundwater flow systems with quasi-steady flow. Hence, if the time interval between two consecutive rainfall events was greater than 2 days, it was reduced to 2 days to construct new rainfall $\delta^{18}O$ ($\delta^{2}H$) time series and amount time series as input and weighting functions, respectively. For the input function, $\delta^{18}O$ ($\delta^{2}H$) values for several lost rainfall samples were calculated according to the regression equation of $\delta^{18}O$ ($\delta^{2}H$) on precipitation amount (Figure 3). Meanwhile, if the time interval between a I-type soil water sampling campaign and its preceding rainfall event was greater than 1.8 days, it was reduced to 1.8 days (a little shorter than 2 days to avoid co-occurrence of the soil water sampling campaign and its subsequent rainfall event in the input and output functions) to construct new soil water $\delta^{18}O$ ($\delta^{2}H$) time series as the output functions. Overall, 266 days were removed from the entire observation period of 438 days. After the elimination of these relatively stagnant periods of intermittent soil water flow, the original flow turned into more steady virtual flow, resulting in an improvement (improvements) in the accuracy of the fitted transport parameter(s). The MTT (τ) of the tracer carried by the virtual flow through a depth roughly represented the lower limit of the MTT (LL_{MTT}) of the tracer through that depth, designated as τ_{LL}, and could be used to calculate the corresponding MTT of the tracer during the entire observation period (T_t), designated as τ_T, as follows:

$$\tau_T = \frac{T_t}{T_t - T_s}\tau_{LL} \tag{9}$$

where T_s was the sum of the stagnant periods during T_t.

The $\delta^{18}O$ ($\delta^{2}H$) time series of I-type soil water for each depth interval was assigned to the corresponding mid-depth. As both piston flow and the mixing effect played a role in I-type soil water percolation (details given in Sections 5.1.2 and 5.1.4), EPM and DM were chosen for the convolution modeling. Equation 3 was used to relate the output isotope tracer to the input tracer. The parameters of the convolution model were found through trial and error to minimize the following least squares statistic:

$$\mathrm{RMSE} = \sqrt{\frac{\sum_{i=1}^{n}(O_i - X_i)^2}{n}} \tag{10}$$

where RMSE represents the square root of the mean square error that evaluates the goodness of fit of the model, O_i is the ith observed output tracer concentration, and X_i is the corresponding value

TABLE 1 Soil particle size distributions for different depth intervals in the planar soil mass type microhabitat in the middle part of a steep hillslope.

Depth interval (cm)	Soil particle size distribution			Soil texture
	Clay (<0.002 mm, %)	Silt (0.002–0.05 mm, %)	Sand (0.05–2 mm, %)	
0 to 10	14.5 ± 1.6	72.0 ± 2.1	13.5 ± 3.6	Silt loam
10 to 20	15.4 ± 1.5	74.9 ± 1.9	9.6 ± 2.9	
20 to 30	16.1 ± 2.1	75.8 ± 2.9	8.1 ± 3.5	
30 to 40	16.7 ± 2.3	76.7 ± 2.2	6.6 ± 1.7	
40 to 50	17.4 ± 1.8	78.5 ± 2.0	4.1 ± 0.3	

Note.Values are means ± standard deviations (n = 3)

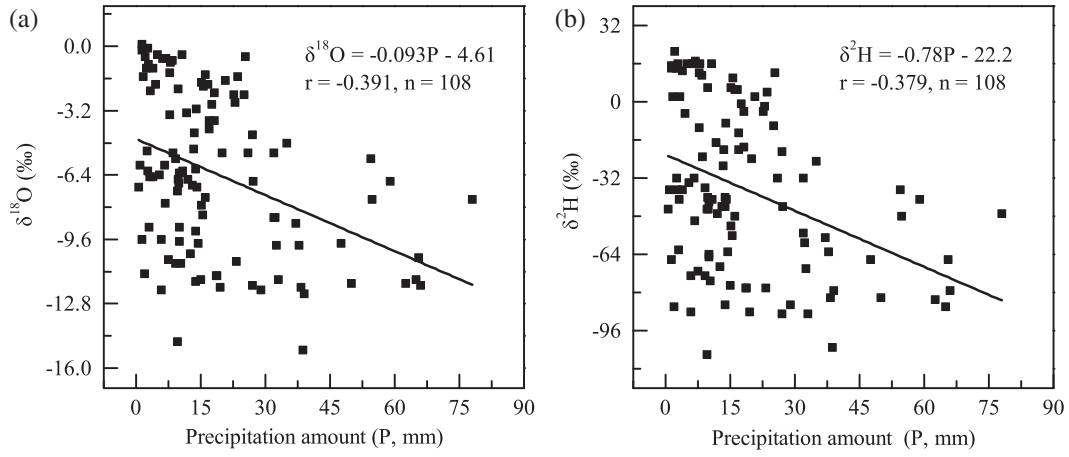

FIGURE 3 Relationships between the amount and (a) $\delta^{18}O$ and (b) $\delta^{2}H$ of precipitation

simulated by the model. This procedure was performed using MATLAB 7 with self-written codes (Weiwei Dai).

To evaluate the validity of our method for estimating the MTT of soil water, we evaluate the sensitivity of the convolution model to different input scenarios, with details given in Supporting Information A. The discussion verified that our method improved the accuracy of the fitted transport parameters.

4 | RESULTS

4.1 | Soil characteristics

The soil texture was silt loam according to the classification defined by the United States Department of Agriculture. The soil clay (silt) content increased from 14.5 ± 1.6 (72.0 ± 2.1) for 0 to 10 cm to 17.4 ± 1.8% (78.5 ± 2.0%) for the 40 to 50 cm depth interval (Table 1), and soil bulk density increased from 1.14 ± 0.05 (2.5 to 7.5 cm) to 1.71 ± 0.06 g/cm^3 (39 to 44 cm) with increasing soil depth (Table 2). Values are means ± standard deviations (n = 3).

4.2 | Hydrogeochemical characteristics of rainfall

Linear regression analysis of rainfall $\delta^{18}O$ and δ^2H values provided the following local meteoric water line (LMWL) equation (Figure 4a):

$$\delta^2H = 8.60\delta^{18}O + 17.75, \left(R^2 = 0.98, n = 108\right). \quad (11)$$

This LMWL was similar to those found in nearby Guilin City (δ^2H = 8.89$\delta^{18}O$ + 18.58, δ^2H = 8.43$\delta^{18}O$ + 16.28; Zhang, Zhu, Wu, Yin, & Pan, 2014b), a Chinese monitoring site incorporated into the Global Network of Isotopes in Precipitation. The significant negative correlation between the amount and $\delta^{18}O$ (δ^2H) of precipitation (p < .01, Figure 3) demonstrated an amount effect on precipitation $\delta^{18}O$ (δ^2H) in this study area. Rainfall $\delta^{18}O$ (δ^2H) values ranged from −15.1 (−106) to −3.3‰ (−17‰) during the summer and varied from −2.9 (−1) to −0.5‰ (21‰) during the winter. They exhibited an obvious seasonal cyclic trend, with superimposed sub-seasonal fluctuations (Figure 5b,c).

4.3 | Hydrogeochemical characteristics of soil water

4.3.1 | I-type soil water

The relationship between $\delta^{18}O$ and δ^2H of I-type soil water is shown in Figure 4b. Precipitation was the only source of soil water in this area, leading to the generally high SVWC during the rainy season (Figure 5a).

TABLE 2 Statistical results of bulk densities (n = 3) for different depth intervals in the planar soil mass type microhabitat in the middle part of a steep hillslope

Depth interval (cm)	Mean (g/cm^3)	Standard deviation (g/cm^3)
2.5 to 7.5	1.14	0.05
12.5 to 17.5	1.30	0.05
22.5 to 27.5	1.46	0.06
32.5 to 37.5	1.65	0.06
39 to 44	1.71	0.06

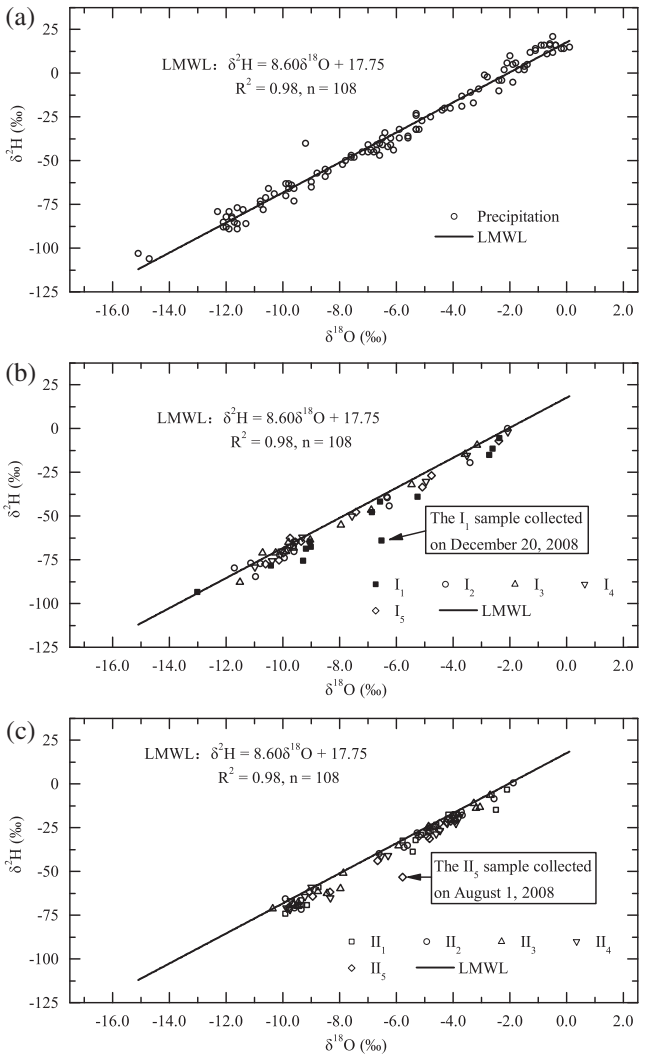

FIGURE 4 Relationships between (a) $\delta^{18}O$ and δ^2H values of rainfall, (b) I-type soil water, and (c) II-type soil water. I_1, I_2, I_3, I_4, and I_5 represent I-type soil water from 0 to 10, 10 to 20, 20 to 30, 30 to 40, and 40 to 43 cm depth intervals, respectively, and II_1, II_2, II_3, II_4, and II_5 denote II-type soil water from 10, 20, 30, 40, and 50 cm depths, respectively

$\delta^{18}O$ (δ^2H) values of I_1, I_2, I_3, I_4, and I_5 ranged from −13.0 (−93) to −2.4 (−5), −11.7 (−85) to −2.1 (0), −11.5 (−88) to −3.2 (−10), −11.0 (−79) to −2.1 (−2), and −10.6 (−77) to −2.4‰ (−7‰), respectively. I-type soil water $\delta^{18}O$ (δ^2H) values for each depth interval roughly exhibited a similar but lagged seasonal cyclic trend as that of rainfall (Figure 5b,c, Table 3), with the corresponding distribution shown in Figure 6.

The vertical profiles of I-type soil water $\delta^{18}O$ (δ^2H) values on November 11, December 20, 2008, January 14, and February 26, 2009, are shown in Figure 7. $\delta^{18}O$ (δ^2H) values for these four profiles

[2]If a soil layer was thick enough, and piston flow was the dominant mechanism for soil water percolation, the seasonal cyclical trend of rainfall $\delta^{18}O$ (δ^2H) values in our study area (Figure 5b,c) would be effectively imitated in the soil profile. We referred to the cyclical tipping points of the soil water isotope profile, which corresponded to the seasonal tipping points of rainfall $\delta^{18}O$ (δ^2H) values, as seasonal tipping points to emphasize the relationship between rainfall and soil water.

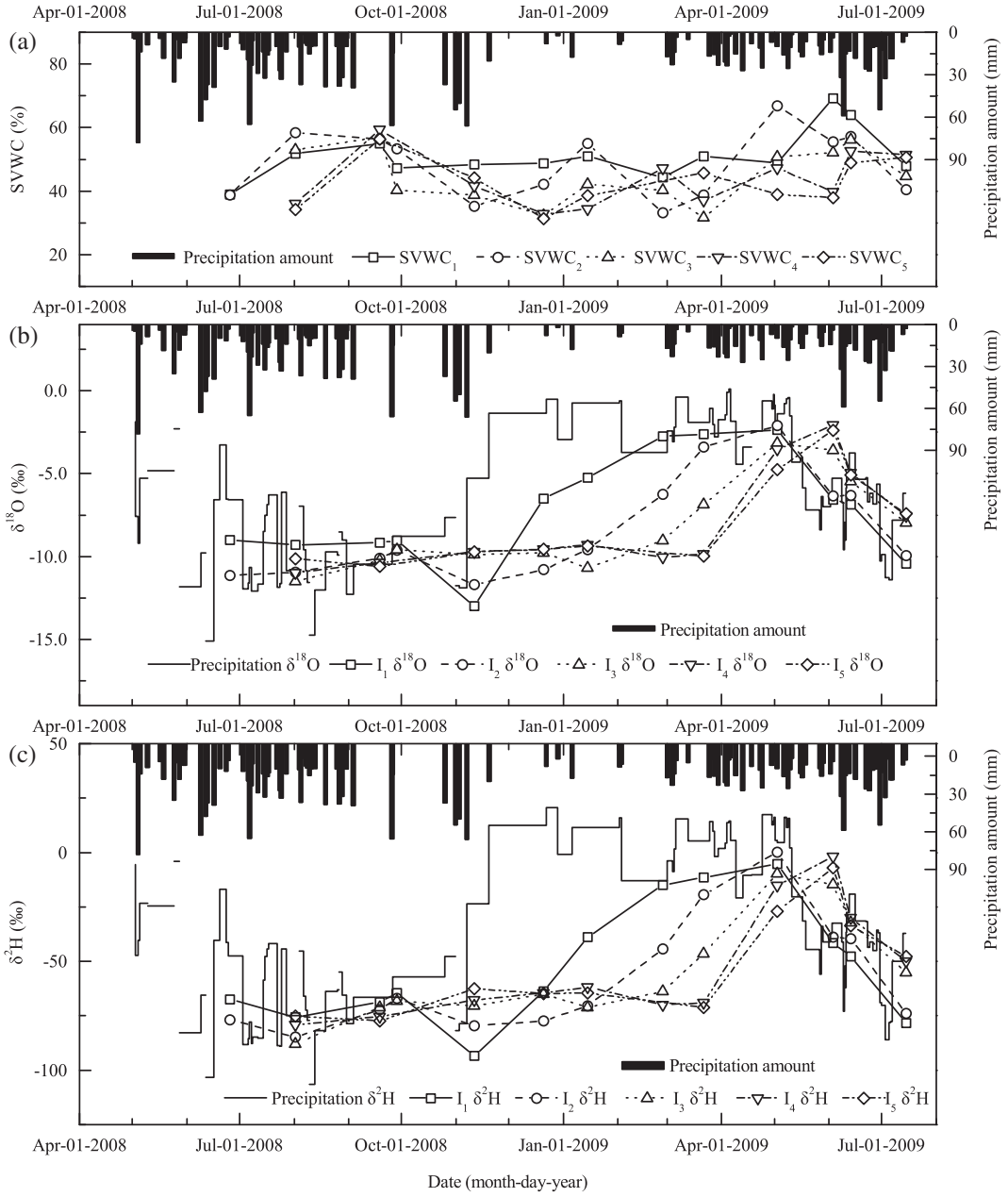

FIGURE 5 Temporal variations in the (a) soil volumetric water content (SVWC), (a, b, and c) precipitation amounts, (b) $\delta^{18}O$, and (c) $\delta^{2}H$ values of rainfall and I-type soil water (designated as I). Subscript numbers 1, 2, 3, 4, and 5 denote 0 to 10, 10 to 20, 20 to 30, 30 to 40, and 40 to 43 cm depth intervals, respectively

TABLE 3 Seasonal tipping points (STPs) and the corresponding lag times of the temporal variations in I-type soil water $\delta^{18}O$ ($\delta^{2}H$) values for different depth intervals, as compared to those of the seasonal trend of rainfall $\delta^{18}O$ ($\delta^{2}H$) values

	The first STP corresponding to the rainfall $\delta^{18}O$ or $\delta^{2}H$ STP in early November 2008		The second STP corresponding to the rainfall $\delta^{18}O$ or $\delta^{2}H$ STP in early May 2009	
$\delta^{18}O$ or $\delta^{2}H$ time series	Date of occurrence	Lag time (month)	Date of occurrence	Lag time (month)
I_1	Early to mid-November 2008	Not obvious	Early May 2009	Not obvious
I_2	Early to mid-November 2008	Not obvious	Early May 2009	Not obvious
I_3	Mid-January 2009	Approximately 2	Early to Mid-May 2009	Approximately 0 to 1
I_4	Mid to late March 2009	Approximately 4	Early June 2009	Approximately 1
I_5	Mid to late March 2009	Approximately 4	Early June 2009	Approximately 1

Note. Here, I_1, I_2, I_3, I_4, and I_5 denote I-type soil water from 0 to 10, 10 to 20, 20 to 30, 30 to 40, and 40 to 43 cm depth intervals, respectively.

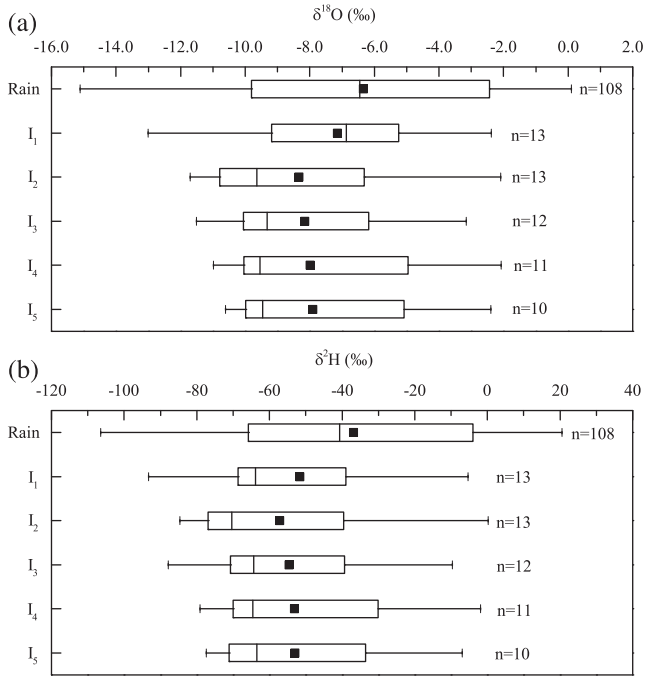

FIGURE 6 Box and whisker plot summarizing the distribution (lower extreme, lower quartile, median, upper quartile, and upper extreme) of (a) $\delta^{18}O$ and (b) $\delta^{2}H$ values of rainfall and I-type soil water. The solid square of each plot represents the mean value of that data set. The number of data for each plot is plotted to its right. I_1, I_2, I_3, I_4, and I_5 denote I-type soil water from 0 to 10, 10 to 20, 20 to 30, 30 to 40, and 40 to 43 cm depth intervals, respectively

ranged from −13.0 (−93) to −9.7 (−62), −10.8 (−77) to −6.5 (−64), −10.7 (−71) to −5.3 (−39), and −10.0 (−70) to −2.7‰ (−15‰), respectively. The downward vertical profile of I-type soil water $\delta^{18}O$ ($\delta^{2}H$) values on November 11, 2008, followed the inverse temporal trend of previous rainfall $\delta^{18}O$ ($\delta^{2}H$) values (data not shown). It was probable that each soil water $\delta^{18}O$ ($\delta^{2}H$) profile in Figure 7 only preserved a part of the seasonal trend of previous rainfall $\delta^{18}O$ ($\delta^{2}H$) values without effectively retaining a seasonal tipping point[2] to show a clear cyclical variation.

The temporal trend of rainfall $\delta^{18}O$ ($\delta^{2}H$) values from May 3 to June 3, 2009, was effectively imitated in the $\delta^{18}O$ ($\delta^{2}H$) vertical profile of I-type soil water on June 3, 2009 (Figure 8, due to the similarities between the $\delta^{18}O$ and $\delta^{2}H$ figures, only the former is shown). The I-type soil water $\delta^{18}O$ ($\delta^{2}H$) values varied from −6.6 (−42) to −2.1‰ (−2‰).

The convolution modeling results are shown in Table 4 and Figure 9. Due to the similarities between the $\delta^{18}O$ and $\delta^{2}H$ figures, only the former is shown. According to the RMSE values, EPM and DM showed comparable suitability for modeling the transport of each tracer through each depth. The LL_{MTT}s of ^{18}O (^{2}H) through each depth based on EPM and DM were roughly comparable to each other and increased with soil depth. The η (D_p) values for ^{18}O and ^{2}H were roughly comparable at each depth. The product of D_p and the corresponding soil depth for ^{18}O (^{2}H) increased from 2.21 cm (1.16 cm) for a 5 cm depth to 10.04 cm (14.37 cm) for a 41.5 cm depth.

As the soil texture was silt loam with only a small content of clay particles (Table 1), the reservoir of immobile water in the soil should

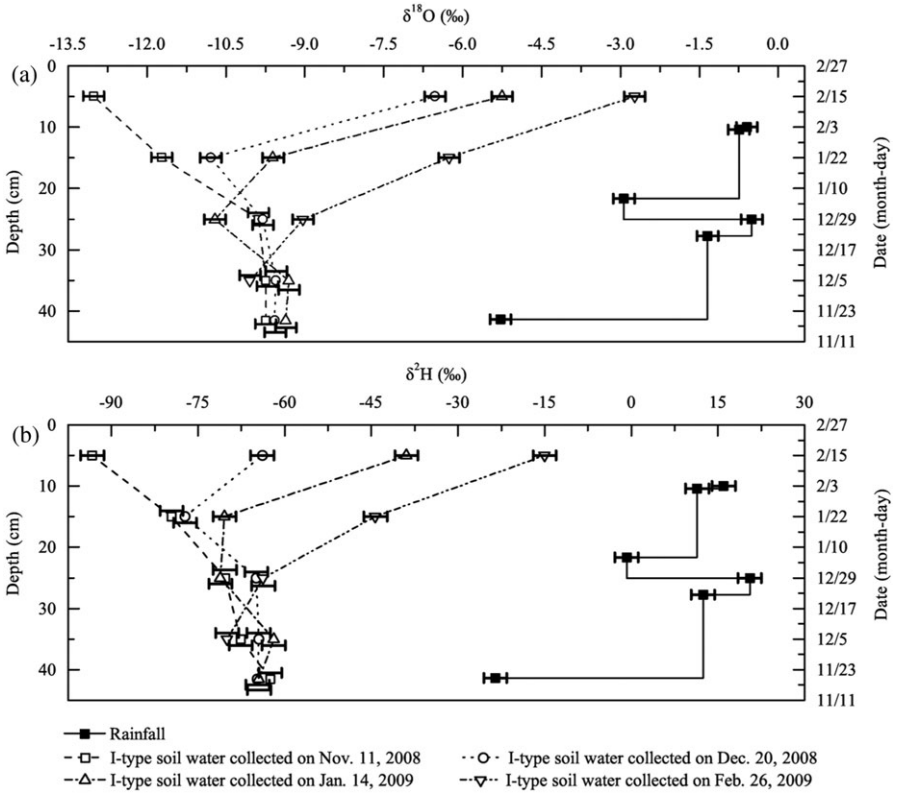

FIGURE 7 Vertical profiles of I-type soil water (a) $\delta^{18}O$ and (b) $\delta^{2}H$ values on November 11 and December 20, 2008, and January 14 and February 26, 2009, as compared to temporal variations in rainfall (a) $\delta^{18}O$ and (b) $\delta^{2}H$ values from November 11, 2008, to February 26, 2009. Error bars represent the analytical precision of the $\delta^{18}O$ or $\delta^{2}H$ determination. Each I-type soil water δ-value was assigned to the corresponding mid-depth

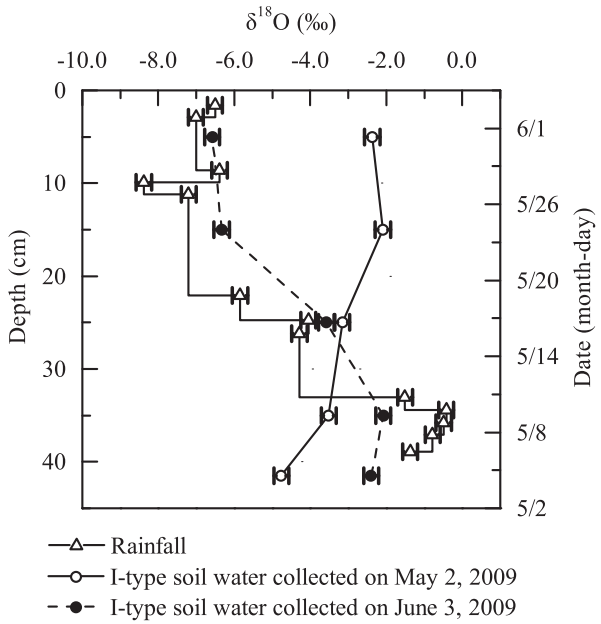

FIGURE 8 Vertical profiles of I-type soil water $\delta^{18}O$ values on May 2 and June 3, 2009, as compared to the temporal variation in rainfall $\delta^{18}O$ values from May 3 to June 3, 2009. Due to the similarities between the $\delta^{18}O$ and $\delta^{2}H$ figures, only the former is shown. Error bars represent the analytical precision of the $\delta^{18}O$ determination. Each I-type soil water $\delta^{18}O$ value was assigned to the corresponding mid-depth

be small. Therefore, the TTDFs of each tracer were assumed to roughly represent those of I-type soil water. Given that EPM and DM showed comparable suitability for modeling the transport of each tracer through each depth, all LL_{MTT}s of ^{18}O and ^{2}H through each depth were averaged to estimate the LL_{MTT} of I-type soil water through that depth, and then the corresponding MTT of I-type soil water for the entire observation period was calculated according to Equation 9 (Table 5). There was a strong positive correlation between LL_{MTT}s (τ_{LL}) of I-type soil water and soil depth (Figure 10):

$$\text{Depth} = 1.55\times\tau_{LL}\left(R^2 = 0.99, n = 5\right) \quad (12)$$

The LL_{MTT} of I-type soil water and its corresponding MTT during the entire observation period increased proportionally with increasing soil depth from 4.81 and 12.25 days through a 5 cm depth to 27.44 and 69.88 days through a 41.5 cm depth, respectively.

The mean percolation rate (MPR) and the total percolation flux of I-type soil water through each depth and the ratio of the latter to the total precipitation flux for the entire observation period were calculated (Table 5), based on the assumption of a complete displacement mechanism for I-type soil water percolation. Except for the 5 cm depth, the values of these three parameters decreased with soil depth.

4.3.2 | II-type soil water

II-type soil water samples were mainly collected during the rainy season, with no sample collected during the winter. During the study period, the total amount of water collected by each zero-tension lysimeter was no more than 83.2 mm (Table 6). The relationship between $\delta^{18}O$ and $\delta^{2}H$ of II-type soil water is shown in Figure 4c. The water amount weighted mean $\delta^{18}O$ ($\delta^{2}H$) value of the water samples collected by each zero-tension lysimeter from May 2008 to July 2009 was no less than the precipitation amount weighted mean $\delta^{18}O$ ($\delta^{2}H$) value of the precipitation samples collected during the same period (Table 7).

For each depth in each plot, the middle time of every two consecutive sampling campaigns was assigned to the latter sample to construct a $\delta^{18}O$ ($\delta^{2}H$) time series of II-type soil water (Figure 11), which could be considered as a weighted moving average time series of the real-time $\delta^{18}O$ ($\delta^{2}H$) variations, with a highly dampened amplitude due to the relatively long sampling interval (approximately 1 month). Each $\delta^{18}O$ ($\delta^{2}H$) time series of II-type soil water roughly exhibited a seasonal cyclic pattern (Figure 11). In Plot 1, $\delta^{18}O$ ($\delta^{2}H$) values of II_1, II_2, II_3, II_4, and II_5 ranged from −9.9 (−74) to −2.1 (−3), −9.9 (−72) to −1.9 (1), −9.6 (−69) to −3.1 (−13), −9.9 (−72) to −3.8 (−17), and −9.8 (−71) to −3.9‰ (−20‰), respectively. In Plot 2, II_3 $\delta^{18}O$ ($\delta^{2}H$) values varied from −10.3 (−71) to −2.7‰ (−6‰).

The $\delta^{18}O$ and $\delta^{2}H$ vertical profiles of II-type soil water collected on August 1 and 7, 2008, in Plot 1 and of I-type soil water collected on August 1, 2008, are shown in Figure 12. During this period, four rainfall events occurred, with the latter two having very small

TABLE 4 Fitted parameters of the exponential-piston flow model (EPM) and dispersion model (DM) for modeling I-type soil water ^{18}O and ^{2}H transport from the soil surface to five different depths after elimination of the relatively stagnant periods of intermittent soil water flow for the time variable

Isotope	Soil depth (*SD*, cm)	Number of data points for the output function	EPM			DM			
			η	τ_{LL} (day)	RMSE	D_p	τ_{LL} (day)	RMSE	D_p**SD* (cm)
^{18}O	5	13	1.61	4.73	1.27	0.442	3.52	1.29	2.21
	15	13	1.49	7.02	0.75	0.196	7.22	0.79	2.94
	25	12	1.26	15.84	0.59	0.248	14.99	0.58	6.21
	35	11	1.57	20.91	0.79	0.151	20.22	0.77	5.29
	41.5	10	1.44	25.02	0.72	0.242	25.01	0.76	10.04
^{2}H	5	13	1.46	5.72	8.05	0.232	5.27	7.89	1.16
	15	13	1.65	8.26	8.57	0.231	8.28	9.54	3.47
	25	12	1.21	17.03	6.45	0.299	16.89	6.92	7.48
	35	11	1.84	24.00	7.73	0.185	22.26	8.23	6.49
	41.5	10	1.35	29.84	8.47	0.346	29.88	8.58	14.37

Note. Here, τ_{LL} and RMSE denote the lower limit of the mean transit time and the square root of the mean square error, respectively. RMSE was calculated according to Equation 10. I-type soil water $\delta^{18}O$ ($\delta^{2}H$) time series for each depth interval was assigned to the corresponding mid-depth.

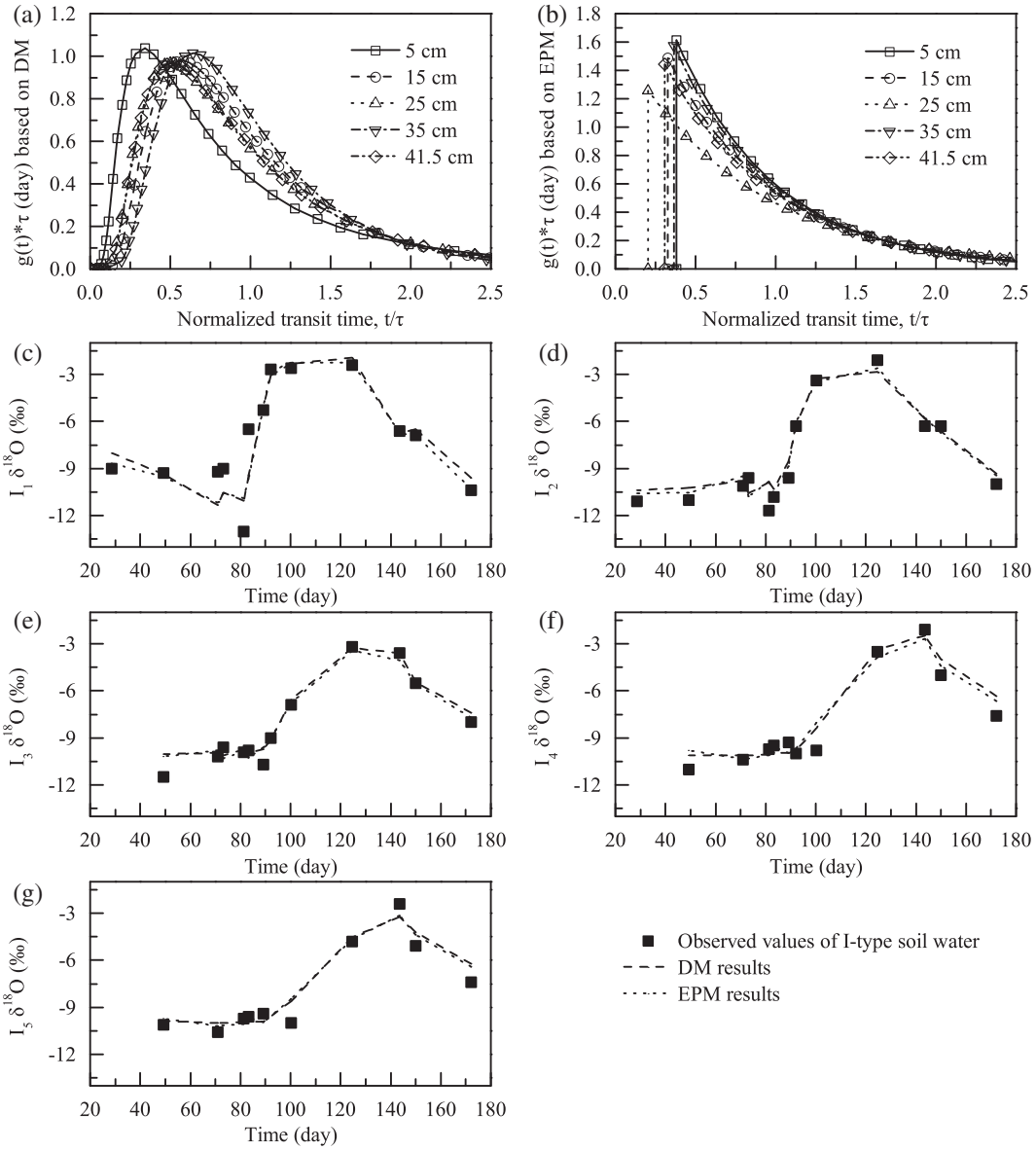

FIGURE 9 Transit time distribution functions, g(t), of the I-type soil water ^{18}O transport from the soil surface to different depths, (a, b) each of which was multiplied by the corresponding mean transit time (τ) and then was plotted against the corresponding normalized transit time (t/τ), and the simulated time series curves versus observed scatter plots of I-type soil water $\delta^{18}O$ values for different depths (c ~ g), based on the exponential-piston flow model (EPM) and dispersion model (DM) after elimination of the relatively stagnant periods of the intermittent soil water flow for the time variable. I_1, I_2, I_3, I_4, and I_5 denote I-type soil water from 0 to 10, 10 to 20, 20 to 30, 30 to 40, and 40 to 43 cm depth intervals, respectively. The $\delta^{18}O$ time series of I-type soil water for each depth interval was assigned to the corresponding mid-depth

TABLE 5 Mean transit times (τ_T), mean percolation rates (MPRs), and total percolation fluxes (TPFs) of I-type soil water through different depths, and the ratios (Rs) of the TPFs to the total precipitation flux for the entire observation period

Soil depth (cm)	τ_{LL} (day)	τ_T (day)	MPR (mm/day)	TPF (mm)	R
5	4.81	12.25	2.09	915	0.42
15	7.70	19.61	3.85	1686	0.77
25	16.19	41.23	2.97	1301	0.59
35	21.85	55.64	2.99	1310	0.60
41.5	27.44	69.88	2.79	1222	0.56

Note. The lower limits of mean transit times (τ_{LL}) of I-type soil water through the corresponding depths were also shown for comparison. τ_T was calculated according to Equation 9. A complete displacement mechanism for I-type soil water percolation was assumed for these calculations.

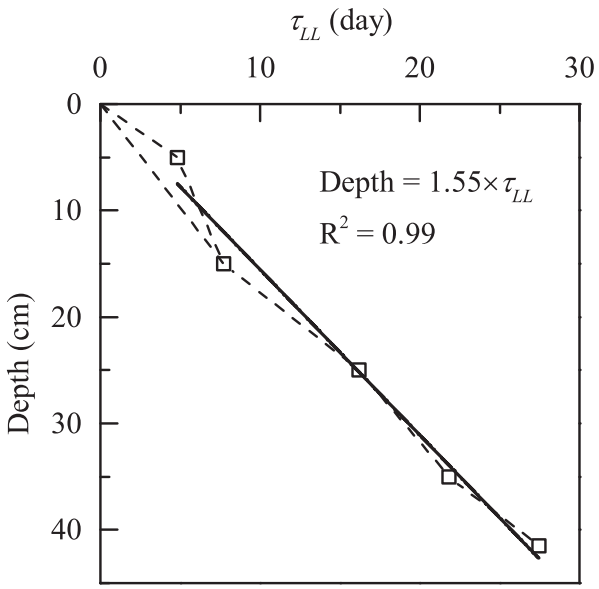

FIGURE 10 The correlation between lower limits of mean transit times (τ_{LL}) of I-type soil water and soil depth. The linear regression line, represented by the solid line, was forced to pass through the origin. The slope of the dashed line connecting two adjacent data points or the origin and the 5-cm (15-cm) depth data point equaled the upper limit of mean flow velocity of I-type soil water passing through the corresponding depth interval

precipitation amounts of 0.6 and 1.4 mm, respectively. The sample of the second rainfall event (August 4, 2008) was lost. All of the potential sources excluding the second rainfall event for the II_3, II_4, and II_5 samples collected on August 7, 2008, were depleted in ^{18}O (^{2}H) by no less than 1.0‰ (10‰) compared to these soil water samples.

5 | DISCUSSION

5.1 | Soil water movement mechanism

5.1.1 | Evapotranspiration

Most points of I-type soil water were located slightly on the right side of the LMWL, except for one I_1 sample collected on December 20, 2008, which deviated obviously to the right of the LMWL (Figure 4b). Thus, the evaporation effect on I-type soil water was generally weak except during the winter when the evaporation effect on the uppermost 10-cm soil matrix water might be significant. Therefore, the decrease in MPR of I-type soil water with soil depth, except for the abnormal lowest MPR through 5 cm, might be mainly caused by transpiration (Table 5). The abnormal MPR might be caused by overestimation of the corresponding MTT of I-type soil water, underestimation of the corresponding average SVWC, and/or preferential flow that bypassed the shallower soil layer but recharged the deeper one.

II-type soil water was mainly composed of the more mobile component of I-type soil water and/or preferential flow. Its samples were all collected during the non-winter period when the evaporation effect on I-type soil water was weak. In addition, the preferential flow, if it occurred, was primarily composed of event water unlikely to be considerably influenced by evaporation. Therefore, the evaporation effect on II-type soil water was weak, and the abnormal data of the II_5 sample collected on August 1, 2008, should be attributed to ineffective preservation of the sample (Figure 4c).

5.1.2 | Vertical piston flow versus lateral flow

The following evidence demonstrated that vertical piston flow played an important role in soil water movement in the planar soil

TABLE 6 The total amount of II-type soil water collected by each zero-tension lysimeter from May 2008 to July 2009

	The total amount (mm) of II-type soil water collected from each depth				
Sampling plot	10 cm	20 cm	30 cm	40 cm	50 cm
1	26.4	83.2	5.0	30.6	22.0
2	NZTL	NZTL	1.0	NZTL	0

Note. NZTL means that there was no zero-tension lysimeter in the plot at that depth. The water amount was expressed as the quotient of the total volume of II-type soil water to the surface area of the collection tray.

TABLE 7 The water amount weighted mean $\delta^{18}O$ ($\delta^{2}H$) value of II-type soil water samples collected by each zero-tension lysimeter from May 2008 to July 2009, as compared to the precipitation amount weighted mean $\delta^{18}O$ ($\delta^{2}H$) value of precipitation samples collected during the same period

	Plot 1		Plot 2		Precipitation	
Depth (cm)	$\delta^{18}O$ (‰)	$\delta^{2}H$ (‰)	$\delta^{18}O$ (‰)	$\delta^{2}H$ (‰)	$\delta^{18}O$ (‰)	$\delta^{2}H$ (‰)
0					−7.7	−48
10	−6.7	−45	NZTL	NZTL		
20	−6.3	−40	NZTL	NZTL		
30	−6.2	−39	−5.9	−34		
40	−7.1	−48	NZTL	NZTL		
50	−6.2	−41	NWS	NWS		

Note. NZTL means that there was no zero-tension lysimeter in the plot at that depth. NWS means that no water sample had been collected from that depth in the plot during the study period.

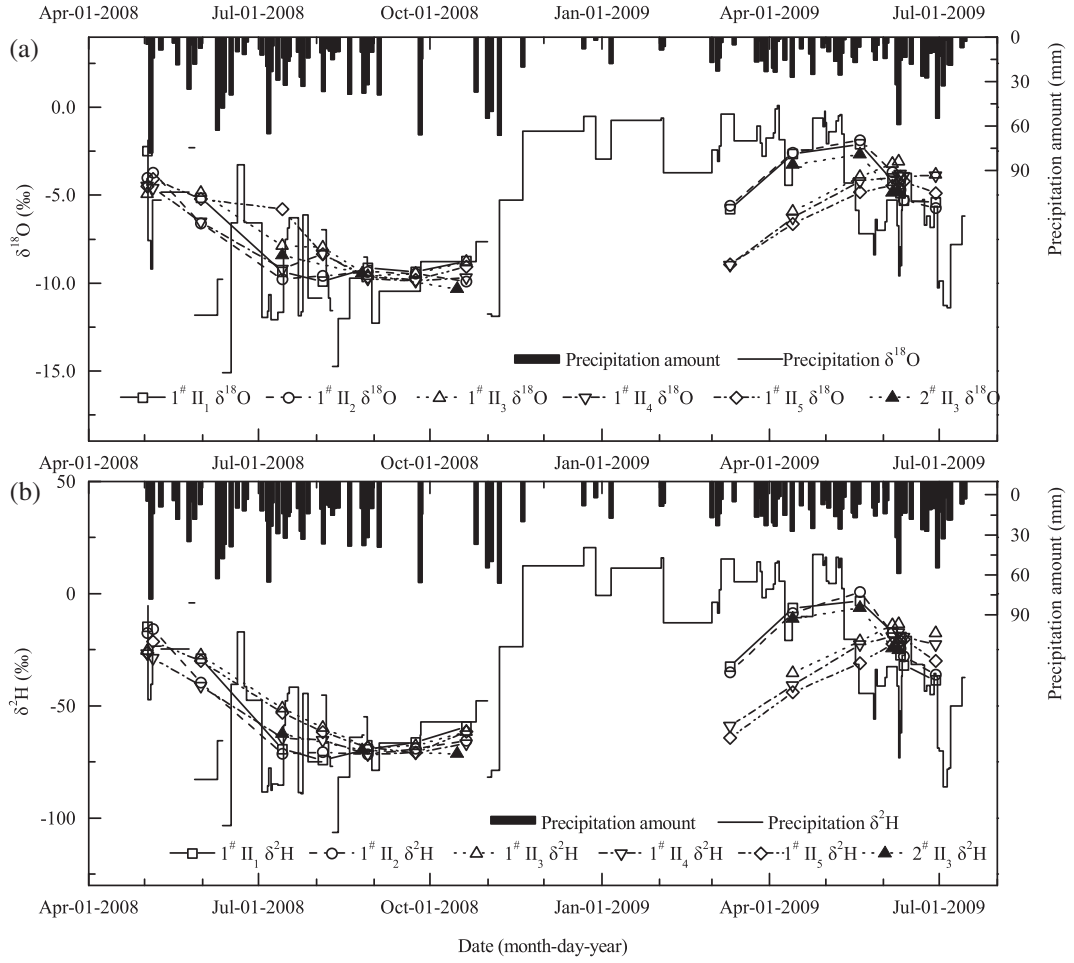

FIGURE 11 (a, b) Temporal variations in precipitation amounts, (a) $\delta^{18}O$ and (b) $\delta^{2}H$ values of rainfall and II-type soil water. Numbers 1 and 2 represent Plots 1 and 2, respectively, and II_1, II_2, II_3, II_4, and II_5 denote II-type soil water from 10, 20, 30, 40, and 50 cm depths, respectively

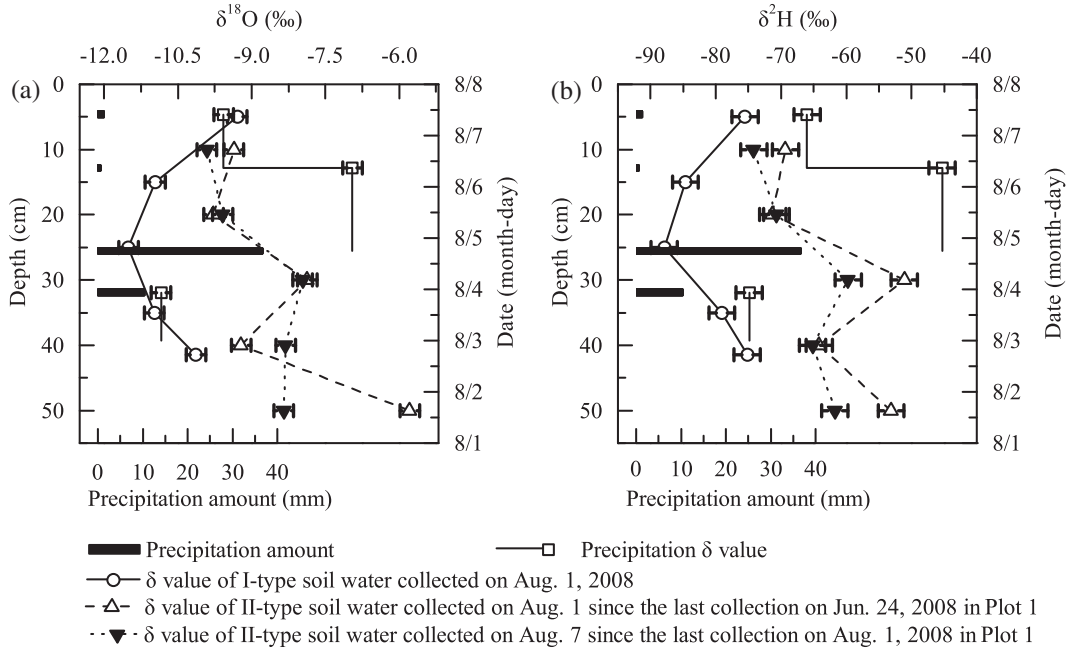

FIGURE 12 (a) $\delta^{18}O$ and (b) $\delta^{2}H$ vertical profiles of II-type soil water collected on August 1 and 7, 2008, in Plot 1 and of I-type soil water collected on August 1, 2008, as compared to temporal variations in (a, b) amounts, (a) $\delta^{18}O$, and (b) $\delta^{2}H$ values of rainfall from August 1 to 7, 2008. Error bars represent the analytical precision of the $\delta^{18}O$ or $\delta^{2}H$ determination. Each I-type soil water $\delta^{18}O$ ($\delta^{2}H$) value was assigned to the corresponding mid-depth

microhabitat. Firstly, the seasonal cyclic variation in I-type soil water $\delta^{18}O$ ($\delta^{2}H$) values for each depth interval lagged the seasonal cyclic trend of precipitation $\delta^{18}O$ ($\delta^{2}H$) values, with a longer lag time for the deeper depth interval (Figure 5b,c, Table 3). Secondly, based on the $\delta^{18}O$ and $\delta^{2}H$ values in Figure 7, the decrease in I_3 $\delta^{18}O$ ($\delta^{2}H$) from December 20, 2008, to January 14, 2009, could be caused only by the isotopically depleted I_2 on December 20, 2008, rather than the isotopically enriched rainfall during this period. Similarly, the decrease in I_4 $\delta^{18}O$ ($\delta^{2}H$) from January 14 to February 26, 2009, should be attributed to the isotopically depleted I_2 and/or I_3 on January 14, 2009, rather than the isotopically enriched rainfall during this period. Thirdly, the temporal trend of rainfall $\delta^{18}O$ ($\delta^{2}H$) values from May 3 to June 3, 2009, was effectively imitated in the $\delta^{18}O$ ($\delta^{2}H$) vertical profile of I-type soil water on June 3, 2009 (Figure 8). Fourthly, there was a strong positive correlation between LL_{MTT}s of I-type soil water and soil depth (Figure 10). Finally, the seasonal tipping points occurring in early to mid-June 2009 for the II_3, II_4, and II_5 $\delta^{18}O$ ($\delta^{2}H$) time series were later than those occurring in mid- to late May 2009 for the II_1 and II_2 $\delta^{18}O$ ($\delta^{2}H$) time series in Plot 1 (Figure 11).

In contrast, the following evidence indicated that lateral flow along the soil–bedrock interface did not play an important role in soil water movement in the upper 43 cm soil layer. Firstly, the amplitude of the $\delta^{18}O$ ($\delta^{2}H$) seasonal variation of I-type soil water for each depth interval was not significantly smaller than that of rainfall (Figures 5b,c and 6), indicating a relatively weak mixing effect on I-type soil water. Secondly, the isotopic signals of rainfall from May 3 to June 3, 2009, were insignificantly attenuated in the lower part of the I-type soil water isotope profiles on June 3, 2009 (Figure 8). Thirdly, there was a strong positive correlation between LL_{MTT}s of I-type soil water and soil depth (Figure 10). Finally, in each plot, the total water amount collected by the deeper zero-tension lysimeter was not considerably different than that collected by the shallower one (Table 6).

The soil layers in Plots 1 and 2 were thicker than 50 cm. Considering that the soil thickness in the planar soil microhabitat was generally less than 50 cm and that the maximum sampling depth of I-type soil water was 43 cm, the above findings actually demonstrated that vertical piston flow, rather than lateral flow along the soil–bedrock interface, played an important role in soil water movement at least in the upper soil layer approximately 7 cm above the permeable bedrock of the planar soil microhabitat in the middle part of the steep hillslope.

Similarly, some water-isotope-based tracing studies had already verified that vertical piston flow could play an important role in soil water movement in thin soil layers overlying permeable bedrock at any position of steep hillslopes (Asano, Uchida, & Ohte, 2002; Uchida, McDonnell, & Asano, 2006), upper hillslopes (even with slope angles of up to 46°) or locations with a weak affinity for saturation (Garvelmann, Külls, & Weiler, 2012; Mueller et al., 2014), and a deep vadose zone of a sandy hill (Gehrels, Peeters, De Vries, & Dekkers, 1998). In contrast, lateral subsurface flow could play an important role in soil water movement in thin soil layers overlying impermeable bedrock in steep hillslopes (Garvelmann et al., 2012; Stewart & McDonnell, 1991; Uchida et al., 2006), foothills, or deep soil layers (Garvelmann et al., 2012; Mueller et al., 2014). Therefore, in regions with steep slopes and thin soil layers, the drainage conditions are key factors for controlling soil water movement.

In this study area, the good drainage conditions, such as the highly fractured and karstified bedrock, the deep groundwater level, and the low soil-clay content (Table 1), facilitated the occurrence of vertical piston flow. In addition, the high SVWC, especially during the rainy season (Figure 5a), also facilitated the occurrence of piston flow in the soil matrix, because many pores of the soil matrix were filled with water under high SVWC and thus served as piston flow pathways during soil water percolation. The high SVWC might be associated with the plentiful rainfall (especially during the rainy season, Figure 5a) and the thin soil layer (generally less than 50 cm) that tended to retain more water per unit volume of soil due to the lack of deep capillary suction. The capillary barrier effect over the soil–bedrock interface would prevent water in the soil with smaller pore sizes from penetrating into the underlying bedrock with larger pore sizes until the water entry pressure for the bedrock was reached (Lee et al., 2007; Ng, Liu, Chen, & Coo, 2015; Ross, 1990) and thus facilitated the occurrence of lateral flow along the interface. However, the fluctuations of the soil–bedrock interface on small scales would probably inhibit the smoothness of lateral flow along the interface in the downslope direction and cause local pooling of lateral flow over local depressions at the interface to facilitate the penetration of lateral flow into the underlying highly fractured and karstified bedrock. In addition, the discontinuous soil layer might also inhibit the continuous development of lateral flow along the soil–bedrock interface.

5.1.3 | Preferential flow

The following evidence suggested that preferential flow could also play a role in soil water movement in the planar soil microhabitat. Firstly, it should be noted that I-type soil water $\delta^{18}O$ ($\delta^{2}H$) decreased from the soil surface to approximately 43 cm depth on November 11, 2008, while the subsequent rainfall from November 11, 2008, to February 26, 2009, was considerably enriched in ^{18}O and ^{2}H (Figure 7). If newer infiltrating water and newer soil water could not bypass older soil water, I-type soil water $\delta^{18}O$ ($\delta^{2}H$) at a certain depth would initially decrease to a minimum and then increase with the percolation of soil water. However, the I_3 $\delta^{2}H$ value initially increased from November 11 to December 20, 2008, and then decreased. Similarly, the I_4 $\delta^{18}O$ ($\delta^{2}H$) value initially increased from November 11, 2008, to January 14, 2009, and then decreased (Figure 7). Secondly, based on the $\delta^{18}O$ and $\delta^{2}H$ data shown in Figure 12, all of the potential sources excluding the second rainfall event for II_3, II_4, and II_5 samples collected on August 7, 2008, in Plot 1 were obviously more depleted in ^{18}O and ^{2}H than these soil water samples. As the evaporation effect on soil water was weak during this period (refer to Section 5.1.1), we can still infer that the second rainfall event was an essential source for these deep soil water samples.

The total amount of water collected by each lysimeter changed irregularly with soil depth in Plot 1, while the total amounts of II-type soil water collected from the same depth in Plots 1 and 2 were considerably different from each other (Table 6). In addition, the temporal variation in II_3 $\delta^{18}O$ ($\delta^{2}H$) values in Plot 1 differed from that in Plot 2, especially during the rainy season in 2009 (Figure 11). Therefore, II-type soil water percolation was spatially heterogeneous, possibly due to preferential flow on a larger scale than the size of the collection tray (400 cm^2).

The high SVWC in the planar soil microhabitat (Figure 5a) facilitated the occurrence of preferential flow because with the increase in SVWC, the soil water pressure increased and could gradually overcome water-entry pressures for macropores to initiate macropore flow or preferential flow, bypassing the soil matrix (Stephens, 1994).

II-type soil water samples, which were only weakly influenced by the evaporation effect (refer to Section 5.1.1), were mainly collected during the rainy season when rainfall $\delta^{18}O$ ($\delta^{2}H$) values were generally lower than those during the dry season (Figure 11). Therefore, given the lower $\delta^{18}O$ ($\delta^{2}H$) values and higher precipitation amounts of rainfall during the rainy season, if II-type soil water was mainly derived from preferential flow, the water amount weighted mean $\delta^{18}O$ ($\delta^{2}H$) value of the water samples collected by each zero-tension lysimeter from May 2008 to July 2009 would be lower than the precipitation amount weighted mean $\delta^{18}O$ ($\delta^{2}H$) value of the precipitation samples collected during the same period. However, the actual calculation gave us the opposite result (Table 7). Therefore, preferential flow had a modest contribution to II-type soil water, which could only be collected by zero-tension lysimeters under saturated conditions (Zhu et al., 2002). In other words, preferential flow played a minor role in soil water percolation under saturated flow conditions, and given this circumstance, it is unlikely that preferential flow played a dominant role in soil water percolation under unsaturated flow conditions.

5.1.4 | Mixing effect

The hydrogeochemical characteristics of soil water showed some evidence of the mixing effect on soil water. Firstly, the amplitude of the seasonal cyclic variation in I-type soil water $\delta^{18}O$ ($\delta^{2}H$) values for each depth interval gradually decreased with soil depth (Figure 5 b, c and 6). Secondly, in Figure 7a, b, with the lowering of the trough of the $\delta^{18}O$ ($\delta^{2}H$) vertical profile of I-type soil water, the trough value gradually increased. Thirdly, the range of the $\delta^{18}O$ ($\delta^{2}H$) values of I-type soil water on June 3, 2009, was narrower than that of rainfall from May 3 to June 3, 2009 (Figure 8). Fourthly, the product of D_p and the corresponding soil depth for each tracer roughly increased with soil depth (Table 4). Finally, the amplitudes of the II_3, II_4, and II_5 $\delta^{18}O$ ($\delta^{2}H$) time series were similar to each other but smaller than those of the II_1 and II_2 $\delta^{18}O$ ($\delta^{2}H$) time series in Plot 1 (Figure 11). The mixing effect on soil water was probably slightly enhanced with soil depth. The mixing effect might be caused by the artificial mixing effect of the I-type soil water sampling method (refer to Section 3.1), mixing of newer infiltrating or percolating water with older soil water, hydrodynamic dispersion, and the interaction between SMF and preferential flow, among other causes. However, it was very hard to identify the dominant factor(s) for the mixing effect based on the water amount and $\delta^{18}O$ and $\delta^{2}H$ data of rainfall and soil water.

5.2 | Implications for the soil water movement characteristics

The soil of the planar soil microhabitat was preliminarily conceptualized as being composed of two zones, that is, the upper vertical percolation zone and the lower lateral flow zone. Because of the good drainage conditions (refer to Section 5.1.2), the vertical percolation zone was probably more important than the lower lateral flow zone.

Soil with a thick vertical percolation zone played an important role in regulating the water cycle at the hillslope. The LL_{MTT} of SMF roughly increased proportionally with soil depth (Figure 10). The thick vertical percolation zone was hard to saturate, inhibiting the occurrence of saturation excess overland flow. This was verified by the fact that, in each plot (whose vertical percolation zone was thicker than 50 cm), the total water amount collected by each zero-tension lysimeter (only collecting saturated water flow) was very low (Table 6), compared to the total percolation flux of I-type soil water (Table 5). The very low-collection efficiency of the zero-tension lysimeter was probably due to the capillary barrier effect (refer to Section 3.1) and the small collection tray area (400 cm^2). The thick vertical percolation zone facilitated infiltration of rainfall. For example, the mean infiltration coefficient of precipitation might be larger than the maximum of the ratios of the total percolation fluxes of I-type soil water to the total precipitation flux, that is, 0.77 (Table 5), in the planar soil microhabitat with a vertical percolation zone thicker than 43 cm, given that preferential flow, which might not be effectively collected by our I-type soil water sampling method, might also contribute to soil water percolation. Overall, the soil thickness was a key factor influencing the capacity of the soil reservoir to regulate the water cycle. For us to better manage and use water resources in this fragile eco-environment, strategies to prevent soil erosion should be implemented. As the vertical piston flow mechanism played a dominant role in soil water percolation, the variation in rainfall $\delta^{18}O$ ($\delta^{2}H$) values over time would be effectively imitated in the soil profile. Therefore, the ^{18}O and/or ^{2}H tracing method can be applied to trace plant water sources and thus can provide insights into utilization of the soil water resource and ecological restoration of degraded ecosystems.

5.3 | Questions and suggestions

This study focused on revealing the characteristics of soil water movement before it reached the soil–bedrock interface of the planar soil microhabitat. In future studies, similar monitoring of soil water isotopic signatures should be performed from the surface to bedrock at different locations along the steep hillslope to provide insights into lateral flow. As neither the soil core collection–vacuum distillation method nor the zero-tension lysimetric method was able to effectively collect unsaturated preferential flow, other soil water sampling methods, such as the wick sampler whose collection efficiency of unsaturated percolating soil water could reach and even exceed 100% (Louie, Shelby, Smesrud, Gatchell, & Selker, 2000; Zhu et al., 2002), should also be employed in the future. The isotopic signatures of groundwater might also provide some information about preferential flow through all of the microhabitats in the hillslope (Gehrels et al., 1998).

Due to the complex micro-topographies of soil and bedrock surfaces in KPCRs, several types of microhabitat can be classified (refer to Section 2). The controlling factors and characteristics of soil water movement in different microhabitats are probably different. We only investigated the soil water movement in the planar soil microhabitat, while the soil water movement in other microhabitats still needs

further investigation. A combination of the isotope tracing method and traditional hydrological methods (e.g., automatic monitoring of the soil water potential) has the potential to considerably improve our understanding of soil water movement.

6 | CONCLUSIONS

By synchronous monitoring of the hydrogeochemical characteristics of rainfall and two types of soil water for more than a hydrological year, the ^{18}O and ^{2}H tracing method was successfully applied to reveal the characteristics of soil water movement in the planar soil microhabitat in the middle of a steep hillslope. Vertical piston flow played an important role in soil water percolation at least in the upper soil layer approximately 7 cm over permeable bedrock. The mixing effect and preferential flow probably also played a role in soil water percolation. The LL_{MTT} of SMF increased proportionally with soil depth. Overall, soil with a thick vertical percolation zone played an important role in regulating the water cycle of the hillslope.

Our study verified that the hydrogeochemical characteristics of different components of soil water that have different integrated degrees of mobility could complement each other to reveal more information about soil water movement. In addition, we proposed a method that improved the accuracy of the estimated soil water MTT based on convolution models. Meanwhile, the MTTs of soil water for different seasons could be estimated. Overall, the isotope tracing method used in this study proved to be a suitable approach for investigating soil water movement in hilly areas with thin soil layers on a monthly scale. This method can also be applied to other areas with similar situations and may be more useful when the information and data about water flow and solute transport processes are limited.

ACKNOWLEDGMENTS

This research work was supported jointly by the National Key Basic Research Program of China (Grant 2013CB956700), the National Key Research Program of China (Grants 2016YFC0502300 and 2016YFC0502602), the NSFC-RCUK_NERC project (Grant 41571130074) and the National Natural Science Foundation of China (Grant 41603001). Professor Jingcheng Ran of the Maolan National Nature Reserve Administration of Libo County in Guizhou Province, China, is acknowledged for his guidance on the field work. The anonymous reviewers are acknowledged for their valuable comments, which greatly helped to improve the manuscript.

REFERENCES

Adomako, D., Maloszewski, P., Stumpp, C., Osae, S., & Akiti, T. T. (2010). Estimating groundwater recharge from water isotope (δ^2H, $\delta^{18}O$) depth profiles in the Densu River basin, Ghana. *Hydrological Sciences Journal*, *55*, 1405–1416. doi:10.1080/02626667.2010.527847

Allison, G. B., & Barnes, C. J. (1983). Estimation of evaporation from non-vegetated surfaces using natural deuterium. *Nature*, *301*, 143–145.

Allison, G. B., Colin-Kaczala, C., Filly, A., & Fontes, J. C. (1987). Measurement of isotopic equilibrium between water, water vapour and soil CO_2 in arid zone soils. *Journal of Hydrology*, *95*, 131–141. doi:10.1016/0022-1694(87)90120-x

Amin, I. E., & Campana, M. E. (1996). A general lumped parameter model for the interpretation of tracer data and transit time calculation in hydrologic systems. *Journal of Hydrology*, *179*, 1–21. doi:10.1016/0022-1694(95)02880-3

Araguás-Araguás, L., Rozanski, K., Gonfiantini, R., & Louvat, D. (1995). Isotope effects accompanying vacuum extraction of soil water for stable isotope analyses. *Journal of Hydrology*, *168*, 159–171.

Asano, Y., Uchida, T., & Ohte, N. (2002). Residence times and flow paths of water in steep unchannelled catchments, Tanakami, Japan. *Journal of Hydrology*, *261*, 173–192. doi:10.1016/s0022-1694(02)00005-7

Barnes, C. J., & Allison, G. B. (1988). Tracing of water movement in the unsaturated zone using stable isotopes of hydrogen and oxygen. *Journal of Hydrology*, *100*, 143–176. doi:10.1016/0022-1694(88)90184-9

Brunel, J.-P., Walker, G. R., & Kennett-Smith, A. K. (1995). Field validation of isotopic procedures for determining sources of water used by plants in a semi-arid environment. *Journal of Hydrology*, *167*, 351–368. doi:10.1016/0022-1694(94)02575-v

Brunel, J. P., Walker, G. R., Dighton, J. C., & Monteny, B. (1997). Use of stable isotopes of water to determine the origin of water used by the vegetation and to partition evapotranspiration. *A case study from HAPEX-Sahel. Journal of Hydrology*, *188-189*, 466–481. doi:10.1016/s0022-1694(96)03188-5

Cao, J., Yuan, D., & Pan, G. (2003). Some soil features in karst ecosystem. *Advance in Earth Sciences*, *18*, 37–44.

Dai, Y., Zheng, X.-J., Tang, L.-S., & Li, Y. (2015). Stable oxygen isotopes reveal distinct water use patterns of two *Haloxylon* species in the Gurbantonggut Desert. *Plant and Soil*, *389*, 73–87. doi:10.1007/s11104-014-2342-z

Dang, H., Chen, H., & Ma, S. (2012). Effects of laminated rock fragments on soil infiltration processes in Karst regions. *Transactions of the Chinese Society of Agricultural Engineering*, *28*, 38–43.

Dansgaard, W. (1964). Stable isotopes in precipitation. *Tellus*, *16*, 436–468. doi:10.1111/j.2153-3490.1964.tb00181.x

Dawson, T. E., & Ehleringer, J. R. (1991). Streamside trees that do not use stream water. *Nature*, *350*, 335–337.

Dawson, T. E., & Ehleringer, J. R. (1993). Isotopic enrichment of water in the "woody" tissues of plants: Implications for plant water source, water uptake, and other studies which use the stable isotopic composition of cellulose. *Geochimica et Cosmochimica Acta*, *57*, 3487–3492. doi:10.1016/0016-7037(93)90554-a

DeWalle, D. R., Edwards, P. J., Swistock, B. R., Aravena, R., & Drimmie, R. J. (1997). Seasonal isotope hydrology of three Appalachian forest catchments. *Hydrological Processes*, *11*, 1895–1906.

Dubbert, M., Cuntz, M., Piayda, A., Maguás, C., & Werner, C. (2013). Partitioning evapotranspiration – Testing the Craig and Gordon model with field measurements of oxygen isotope ratios of evaporative fluxes. *Journal of Hydrology*, *496*, 142–153. doi:10.1016/j.jhydrol.2013.05.033

Ehleringer, J. R., & Dawson, T. E. (1992). Water uptake by plants: Perspectives from stable isotope composition. *Plant, Cell & Environment*, *15*, 1073–1082. doi:10.1111/j.1365-3040.1992.tb01657.x

Figueroa-Johnson, M., Tindall, J., & Friedel, M. (2007). A comparison of $^{18}O\delta$ composition of water extracted from suction lysimeters, centrifugation, and azeotropic distillation. *Water, Air, & Soil Pollution*, *184*, 63–75.

Gan, T., & Mu, B. (1987). A report on the investigation of the Maolan karst forest climate. In Z. Zhou (Ed.), *Scientific survey of the Maolan karst forest* (pp. 98–110). Guiyang in Guizhou Province of China: Guizhou People's Publishing House.

Garvelmann, J., Külls, C., & Weiler, M. (2012). A porewater-based stable isotope approach for the investigation of subsurface hydrological processes. *Hydrology and Earth System Sciences*, *16*, 631–640. doi:10.5194/hess-16-631-2012

Gat, J. R., Mook, W. G., & Meijer, H. A. J. (2001). Observed isotope effects in precipitation. In J. R. Gat, W. G. Mook, & H. A. J. Meijer (Eds.), *Environmental isotopes in the hydrological cycle, principles and applications, vol. 2 atmospheric water* (pp. 197–207). Vienna/Paris: International

Atomic Energy Agency and United Nations Educational, Scientific and Cultural Organization (reprinted with minor corrections).

Gazis, C., & Feng, X. (2004). A stable isotope study of soil water: evidence for mixing and preferential flow paths. *Geoderma*, *119*, 97–111.

Gehrels, J. C., Peeters, J. E. M., De Vries, J. J., & Dekkers, M. (1998). The mechanism of soil water movement as inferred from ^{18}O stable isotope studies. *Hydrological Sciences Journal*, *43*, 579–594.

Hsieh, J. C. C., Savin, S. M., Kelly, E. F., & Chadwick, O. A. (1998). Measurement of soil-water $\delta^{18}O$ values by direct equilibration with CO_2. *Geoderma*, *82*, 255–268. doi:10.1016/s0016-7061(97)00104-3

Ingraham, N. L., & Shadel, C. (1992). A comparison of the toluene distillation and vacuum/heat methods for extracting soil water for stable isotopic analysis. *Journal of Hydrology*, *140*, 371–387. doi:10.1016/0022-1694(92)90249-u

Jemison, J. M. J., & Fox, R. H. (1992). Estimation of zero-tension pan lysimeter collection efficiency. *Soil Science*, *154*, 85–94.

Jiang, T., Wei, C., Xie, D., Xiao, H., Xia, J., & Deng, Y. (2006). Study on water holding capacity of yellow soil in karst area of central Guizhou. *Journal of Soil and Water Conservation*, *20*, 25–29.

Jódar, J., Lambán, L. J., Medina, A., & Custodio, E. (2014). Exact analytical solution of the convolution integral for classical hydrogeological lumped-parameter models and typical input tracer functions in natural gradient systems. *Journal of Hydrology*, *519* (Part D), 3275–3289. doi:10.1016/j.jhydrol.2014.10.027

Landon, M. K., Delin, G. N., Komor, S. C., & Regan, C. P. (1999). Comparison of the stable-isotopic composition of soil water collected from suction lysimeters, wick samplers, and cores in a sandy unsaturated zone. *Journal of Hydrology*, *224*, 45–54.

Lee, K.-S., Kim, J.-M., Lee, D.-R., Kim, Y., & Lee, D. (2007). Analysis of water movement through an unsaturated soil zone in Jeju Island, Korea using stable oxygen and hydrogen isotopes. *Journal of Hydrology*, *345*, 199–211. doi:10.1016/j.jhydrol.2007.08.006

Li, Y., Gao, M., Wei, C., Xie, D., & Liu, G. (2003). Differences of soil water characteristics under different land use patterns in karst mountains. *Journal of Soil and Water Conservation*, *17*, 63–66.

Li, X., Chen, X., Zhou, L., & Fang, K. (2008). Soil moisture characteristics and their affecting factors in the rocky desertification process of karst regions, Southwest China. *Journal of Soil and Water Conservation*, *22*, 198–203.

Liao, H., Long, J., Li, J., Yang, J., & Feng, Y. (2012). Distribution characteristics of soil carbon and nitrogen under different vegetation types in micro-habitats of karst dry-hot valley region of south western China. *Soils*, *44*, 421–428.

Liu, H., Jiang, T., Liu, H., Xiao, H., & Xia, J. (2005). Impact of land use on spatio-temporal variation of soil moisture of sloping upland in karst mountainous area. *Acta Pedologica Sinica*, *42*, 428–433.

Liu, F., Wang, S., Luo, H., Liu, Y., & Liu, H. (2008). Micro-habitats in karst forest ecosystem and variability of soils. *Acta Pedologica Sinica*, *45*, 1055–1062.

Louie, M. J., Shelby, P. M., Smesrud, J. S., Gatchell, L. O., & Selker, J. S. (2000). Field evaluation of passive capillary samplers for estimating groundwater recharge. *Water Resources Research*, *36*, 2407–2416. doi:10.1029/2000wr900135

Małoszewski, P., & Zuber, A. (1982). Determining the turnover time of groundwater systems with the aid of environmental tracers: 1. *Models and their applicability*. *Journal of Hydrology*, *57*, 207–231. doi:10.1016/0022-1694(82)90147-0

Małoszewski, P., & Zuber, A. (1985). On the theory of tracer experiments in fissured rocks with a porous matrix. *Journal of Hydrology*, *79*, 333–358. doi:10.1016/0022-1694(85)90064-2

Małoszewski, P., & Zuber, A. (1996). Lumped parameter models for the interpretation of environmental tracer data. *Manual on Mathematical Models in Isotope Hydrology*, *IAEA-TECDOC*, *910*, 9–58.

Mao, Z., & Zhang, B. (1987). The geological characteristics of the Maolan karst forest. In Z. Zhou (Ed.), *Scientific survey of the Maolan karst forest* (pp. 24–41). Guiyang in Guizhou Province of China: Guizhou People's Publishing House.

Martinec, J., Siegenthaler, U., Oeschger, H., & Tongiorgi, E. (1974). New insights into the runoff mechanism by environmental isotopes. In: Isotope Techniques in Groundwater Hydrology. In: Proceedings of a symposium organized by the International Atomic Energy Agency and held in Vienna, 11-15 March 1974., International Atomic Energy Agency pp: 129–143.

McGuire, K. J., & McDonnell, J. J. (2006). A review and evaluation of catchment transit time modeling. *Journal of Hydrology*, *330*, 543–563. doi:10.1016/j.jhydrol.2006.04.020

McGuire, K. J., DeWalle, D. R., & Gburek, W. J. (2002). Evaluation of mean residence time in subsurface waters using oxygen-18 fluctuations during drought conditions in the mid-Appalachians. *Journal of Hydrology*, *261*, 132–149. doi:10.1016/s0022-1694(02)00006-9

Mueller, M. H., Alaoui, A., Kuells, C., Leistert, H., Meusburger, K., Stumpp, C., … Alewell, C. (2014). Tracking water pathways in steep hillslopes by $\delta^{18}O$ depth profiles of soil water. *Journal of Hydrology*, *519* (Part A), 5340–5352. doi:10.1016/j.jhydrol.2014.07.031

Ng, C. W. W., Liu, J., Chen, R., & Coo, J. L. (2015). Numerical parametric study of an alternative three-layer capillary barrier cover system. *Environmental Earth Sciences*, *74*, 4419–4429. doi:10.1007/s12665-015-4462-z

Peters, A., & Durner, W. (2009). Large zero-tension plate lysimeters for soil water and solute collection in undisturbed soils. *Hydrology and Earth System Sciences*, *13*, 1671–1683. doi:10.5194/hess-13-1671-2009

Ross, B. (1990). The diversion capacity of capillary barriers. *Water Resources Research*, *26*, 2625–2629. doi:10.1029/WR026i010p02625

Rothfuss, Y., Vereecken, H., & Brüggemann, N. (2013). Monitoring water stable isotopic composition in soils using gas-permeable tubing and infrared laser absorption spectroscopy. *Water Resources Research*, *49*, 3747–3755. doi:10.1002/wrcr.20311

Shanafield, M., Cook, P. G., Gutiérrez-Jurado, H. A., Faux, R., Cleverly, J., & Eamus, D. (2015). Field comparison of methods for estimating groundwater discharge by evaporation and evapotranspiration in an arid-zone playa. *Journal of Hydrology*, *527*, 1073–1083. doi:10.1016/j.jhydrol.2015.06.003

Stephens, D. B. (1994). A perspective on diffuse natural recharge mechanisms in areas of low precipitation. *Soil Science Society of America Journal*, *58*, 40–48. doi:10.2136/sssaj1994.03615995005800010006x

Stewart, M. K., & McDonnell, J. J. (1991). Modeling base flow soil water residence times from deuterium concentrations. *Water Resources Research*, *27*, 2681–2693. doi:10.1029/91WR01569

Stumpp, C., & Hendry, M. J. (2012). Spatial and temporal dynamics of water flow and solute transport in a heterogeneous glacial till: The application of high-resolution profiles of $\delta^{18}O$ and $\delta^{2}H$ in pore waters. *Journal of Hydrology*, *438–439*, 203–214. doi:10.1016/j.jhydrol.2012.03.024

Stumpp, C., & Maloszewski, P. (2010). Quantification of preferential flow and flow heterogeneities in an unsaturated soil planted with different crops using the environmental isotope $\delta^{18}O$. *Journal of Hydrology*, *394*, 407–415. doi:10.1016/j.jhydrol.2010.09.014

Stumpp, C., Maloszewski, P., Stichler, W., & Fank, J. (2009a). Environmental isotope ($\delta^{18}O$) and hydrological data to assess water flow in unsaturated soils planted with different crops: Case study lysimeter station "Wagna" (Austria). *Journal of Hydrology*, *369*, 198–208. doi:10.1016/j.jhydrol.2009.02.047

Stumpp, C., Nützmann, G., Maciejewski, S., & Maloszewski, P. (2009b). A comparative modeling study of a dual tracer experiment in a large lysimeter under atmospheric conditions. *Journal of Hydrology*, *375*, 566–577. doi:10.1016/j.jhydrol.2009.07.010

Stumpp, C., Stichler, W., & Maloszewski, P. (2009c). Application of the environmental isotope $\delta^{18}O$ to study water flow in unsaturated soils planted with different crops: Case study of a weighable lysimeter from the research field in Neuherberg, Germany. *Journal of Hydrology*, *368*, 68–78. doi:10.1016/j.jhydrol.2009.01.027

Stumpp, C., Stichler, W., Kandolf, M., & Šimůnek, J. (2012). Effects of land cover and fertilization method on water flow and solute transport in five lysimeters: A long-term study using stable water isotopes. *Vadose Zone Journal*, *11*. doi:10.2136/vzj2011.0075

Sturm, P., & Knohl, A. (2010). Water vapor δ^2H and $\delta^{18}O$ measurements using off-axis integrated cavity output spectroscopy. *Atmospheric Measurement Techniques*, *3*, 67–77. doi:10.5194/amt-3-67-2010

Sun, C., Wang, S., Liu, X., & Feng, Z. (2002). Geochemical characteristics and formation mechanism of rock-soil interface in limestone weathering crust at Huaxi, Guizhou Province. *Acta Mineralogica Sinica*, *22*, 126–132.

Turnadge, C., & Smerdon, B. D. (2014). A review of methods for modelling environmental tracers in groundwater: Advantages of tracer concentration simulation. *Journal of Hydrology*, *519* (Part D), 53674–53689. doi:10.1016/j.jhydrol.2014.10.056

Uchida, T., McDonnell, J. J., & Asano, Y. (2006). Functional intercomparison of hillslopes and small catchments by examining water source, flowpath and mean residence time. *Journal of Hydrology*, *327*, 627–642. doi:10.1016/j.jhydrol.2006.02.037

Veihmeyer, F. J., & Hendrickson, A. H. (1931). The moisture equivalent as a measure of the field capacity of soils. *Soil Science*, *32*, 181–193.

Volkmann, T. H. M., & Weiler, M. (2014). Continual in situ monitoring of pore water stable isotopes in the subsurface. *Hydrology and Earth System Sciences*, *18*, 1819–1833. doi:10.5194/hess-18-1819-2014

Vuille, M., Werner, M., Bradley, R. S., & Keimig, F. (2005). Stable isotopes in precipitation in the Asian monsoon region. *Journal of Geophysical Research: Atmospheres*, *110*. doi:10.1029/2005JD006022.D23108

Walker, C. D., & Richardson, S. B. (1991). The use of stable isotopes of water in characterising the source of water in vegetation. *Chemical Geology: Isotope Geoscience section*, *94*, 145–158. doi:10.1016/0168-9622(91)90007-j

Wang, X.-F., & Yakir, D. (2000). Using stable isotopes of water in evapotranspiration studies. *Hydrological Processes*, *14*, 1407–1421.

Wang, S., Lu, H., Zhou, Y., Xie, L., & Da, X. (2007). Spatial variability of soil organic carbon and representative soil sampling method in Maolan karst virgin forest. *Acta Pedologica Sinica*, *44*, 475–483.

Wang, L., Caylor, K. K., & Dragoni, D. (2009). On the calibration of continuous, high-precision $\delta^{18}O$ and δ^2H measurements using an off-axis integrated cavity output spectrometer. *Rapid Communications in Mass Spectrometry*, *23*, 530–536. doi:10.1002/rcm.3905

Wang, P., Song, X., Han, D., Zhang, Y., & Liu, X. (2010). A study of root water uptake of crops indicated by hydrogen and oxygen stable isotopes: A case in Shanxi Province, China. *Agricultural Water Management*, *97*, 475–482. doi:10.1016/j.agwat.2009.11.008

Weiler, M., McGlynn, B. L., McGuire, K. J., & McDonnell, J. J. (2003). How does rainfall become runoff? A combined tracer and runoff transfer function approach. *Water Resources Research*, *39*, 1315. doi:10.1029/2003WR002331

West, A. G., Patrickson, S. J., & Ehleringer, J. R. (2006). Water extraction times for plant and soil materials used in stable isotope analysis. *Rapid Communications in Mass Spectrometry*, *20*, 1317–1321. doi:10.1002/rcm.2456

Williams, A. E. (1997). Stable isotope tracers: Natural and anthropogenic recharge, Orange County, California. *Journal of Hydrology*, *201*, 230–248.

Yang, B., Wen, X., & Sun, X. (2015). Seasonal variations in depth of water uptake for a subtropical coniferous plantation subjected to drought in an East Asian monsoon region. *Agricultural and Forest Meteorology*, *201*, 218–228. doi:10.1016/j.agrformet.2014.11.020

Yuan, D. (1997). Rock desertification in the subtropical karst of South China. *Z. Geomorph. N. F.*, *108*, 81–90.

Zhang, J., Chen, H., Su, Y., Zhang, W., & Kong, X. (2008). Spatial variability of soil moisture in surface layer in depressed karst region and its scale effect. *Acta Pedologica Sinica*, *45*, 544–549.

Zhang, Z., Zhu, Z., Wang, Y., Fu, W., & Wen, Z. (2010). Soil infiltration capacity and its influencing factors of different land use types in Karst slope. *Transactions of the Chinese Society of Agricultural Engineering*, *26*, 71–76.

Zhang, J., Su, Y., Chen, H., Kong, X., Zhang, W., Zhang, J., & Shen, G. (2014a). Research on spatial distribution and influencing factor of soil moisture in typical depression area of karst region. *Acta Ecologica Sinica*, *34*, 3405–3413.

Zhang, M., Zhu, X., Wu, X., Yin, J., & Pan, M. (2014b). $\delta^{18}O$ characteristics of meteoric precipitation and its water vapor sources in the Guilin area of China. *Environmental Earth Sciences*, 1–24. doi:10.1007/s12665-014-3827-z

Zhu, Y., Fox, R. H., & Toth, J. D. (2002). Leachate collection efficiency of zero-tension pan and passive capillary fiberglass wick lysimeters soil sci. *Soil Science Society of America Journal*, *66*, 37–43.

Zuber, A. (1986a). Chapter 1 - Mathematical models for the interpretation of environmental radioisotopes in groundwater systems. In P. Fritz, & J. C. Fontes (Eds.), *Handbook of Environmental isotope geochemistry Volume 2 The Terrestrial Environment*, *B* (pp. 1–59). Amsterdam of the Netherlands: Elsevier.

Zuber, A. (1986b). On the interpretation of tracer data in variable flow systems. *Journal of Hydrology*, *86*, 45–57. doi:10.1016/0022-1694(86)90005-3

Zuber, A., & Małoszewski, P. (2001). 2 Lumped parameter models. In W. G. Mook, & Y. Yurtsever (Eds.), *Environmental isotopes in the hydrological cycle: Principles and applications* (pp. 5–35). Paris/Vienna: UNESCO/IAEA.

SUPPORTING INFORMATION

Additional Supporting Information may be found online in the supporting information tab for this article.

How to cite this article: Liu W, Wang S, Luo W, Dai W, Bai E. Characteristics of soil water movement in a grass slope in a karst peak-cluster region, China. *Hydrological Processes*. 2017;**31**:1331–1348. https://doi.org/10.1002/hyp.11105